

BRNO UNIVERSITY OF TECHNOLOGY

VYSOKÉ UČENÍ TECHNICKÉ V BRNĚ

FACULTY OF MECHANICAL ENGINEERING

FAKULTA STROJNÍHO INŽENÝRSTVÍ

INSTITUTE OF PHYSICAL ENGINEERING

ÚSTAV FYZIKÁLNÍHO INŽENÝRSTVÍ

MAGNETIC SPIN ICE STATES IN ARTIFICIAL MAGNETIC FRUSTRATED SYSTEMS

MAGNETICKÉ STAVY SPINOVÉHO LEDU V UMĚLÝCH MAGNETICKY FRUSTROVANÝCH SYSTÉMECH

MASTER'S THESIS

DIPLOMOVÁ PRÁCE

AUTHOR

AUTOR PRÁCE

Bc. Vojtěch Schánilec

SUPERVISOR

VEDOUČÍ PRÁCE

Nicolas Rougemaille

BRNO 2018

Master's Thesis Assignment

Institut: Institute of Physical Engineering
Student: **Bc. Vojtěch Schánilec**
Degree program: Applied Sciences in Engineering
Branch: Physical Engineering and Nanotechnology
Supervisor: **Nicolas Rougemaille**
Academic year: 2017/18

As provided for by the Act No. 111/98 Coll. on higher education institutions and the BUT Study and Examination Regulations, the director of the Institute hereby assigns the following topic of Master's Thesis:

Magnetic spin ice states in artificial magnetic frustrated systems

Brief description:

Artificial systems are often used in physics to induce, explore and manipulate intriguing properties of matter, which do not exist in nature or which can be challenging to investigate otherwise. In condensed matter magnetism, artificial arrays of interacting nanomagnets were introduced as a possible way to fabricate experimentally various types of frustrated spin models. These magnetic systems allow to visualize unconventional magnetic phases and exotic collective phenomena directly in real space.

The diploma thesis will contribute to finding the experimental signatures of fragmentation of magnetism in kagome arrays of nanomagnets and to investigating the associated many-body physics.

Master's Thesis goals:

1. Review the state-of-the-art.
2. Design and fabricate 2d arrays of magnetic nanostructures in the magnetically frustrated geometry.
3. Develop an automated procedure for analysis of spin ice configurations obtained by magnetic force microscopy imaging.

Recommended bibliography:

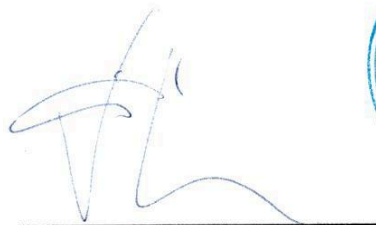
NISOLI, C., MOESSNER, R. a SCHIFFER, P., Colloquium: Artificial spin ice: Designing and imaging magnetic frustration. *Reviews of Modern Physics*, vol. 85, pp. 1473, DOI: 10.1103/RevModPhys.85.1473, 2013.

WANG, R. F. a kol., Artificial 'spin ice' in a geometrically frustrated lattice of nanoscale ferromagnetic islands. *Nature*, vol. 439, pp. 303, DOI: 10.1038/nature04447, 2006.

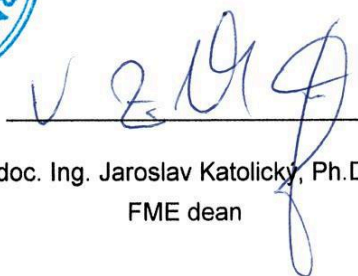
PERRIN, Y., CANALS, B. a ROUGEMAILLE, N., Extensive degeneracy, Coulomb phase and magnetic monopoles in artificial square ice. Nature, vol. 540, pp. 410, DOI: 10.1038/nature20155, 2016.

Students are required to submit the thesis within the deadlines stated in the schedule of the academic year 2017/18.

In Brno, 8. 11. 2017



prof. RNDr. Tomáš Šikola, CSc.
Director of the Institute



doc. Ing. Jaroslav Katolický, Ph.D.
FME dean

Abstract

Artificially spin-ice systems are an appropriate tool for exploring unusual phenomena that are hard to observe in nature. A special case of artificial spin ice system is a kagome lattice that allows you to examine the collective behaviour of spin in the matter. This system has a number of predicted exotic magnetic phases that have not yet been measured and investigated in real space. In this work, we deal with the modification of the kagome lattice so that it can be used to study exotic states in real space. Experiments performed on our modified lattice indicate that we are able to detect both low and high energy states, and therefore the proposed modification of the kagome lattice is suitable for exploring its exotic states in real space.

Abstrakt

Uměle vytvořené systémy spinového ledu jsou vhodným nástrojem pro zkoumání neobvyklých jevů, které se v přírodě dají jen těžko pozorovat. Speciálním případem umělého spinového ledu je kagome mřížka, která umožňuje zkoumat kolektivní chování spinů v látce. Tento systém má řadu předpovězených exotických magnetických fází, které zatím nebyly změřeny a prozkoumány v reálném prostoru. V rámci této práce se zabýváme úpravou kagome mřížky tak, aby mohla být využita ke zkoumání exotických stavů v reálném prostoru. Experimenty provedené na naší upravené mřížce ukazují, že jsme schopni detekovat nízko i vysoko energetické stavy, a tedy, že námi navržená úprava kagome mřížky je vhodná pro zkoumání exotických stavů v reálném prostoru.

Klíčová slova

geometrická frustrace, umělé systémy spinového ledu, kagome mřížka, nízkoenergetické stavy, mikromagnetismus, fragmentace, mikroskopie magnetických sil

Keywords

geometrical frustration, artificial spin ice systems, kagome lattice, low energy states, micromagnetism, fragmentation, magnetic force microscopy

SCHÁNILEC, V. *Magnetic spin ice states in artificial magnetic frustrated systems*. Brno: Brno University of Technology, Faculty of Mechanical Engineering, 2018. 46 p. Supervised by Dr. Nicolas Rougemaille.

DECLARATION

I hereby declare that I have written my master's thesis on the theme of *Magnetic spin ice states in artificial magnetic frustrated systems* independently, under the guidance of the master's thesis supervisor, Dr. Nicolas Rougemaille, and using the technical literature and other sources of information which are all properly quoted in the thesis and detailed in the list of literature at the end of the thesis.

In Brno

.....

(author)

ACKNOWLEDGEMENT

I would like to thank my supervisor Dr. Nicolas Rougemaille for his guidance and inspiring comments. I would like to express my gratitude to Dr. Vojtěch Uhlíř who supported me greatly and taught me what matters in science and in life. Special thanks belong to Lukáš Flajšman who is always available to help if the need arise. Thank all my colleagues from the micromagnetic group for all discussions about magnetism and related topics. My gratitude definitely belongs to my family for their support during all these years, especially to my fiancée Gabriela Olivíková, who always provide me with unfailing support.

This work was carried out with the support of CEITEC Nano Research Infrastructure (ID LM2015041, MEYS CR, 2016–2019), CEITEC Brno University of Technology.

Bc. Vojtěch Schánilec

Contents

1	Preamble	3
2	Artificial spin ice systems	4
2.1	Background	4
2.1.1	The three main phases of matter	4
2.1.2	Link with the third law of thermodynamics	5
2.1.3	Geometrically frustrated systems	6
2.1.4	From ice to spin ice	9
2.2	Ising spin lattice models	10
2.2.1	Square lattice	10
2.2.2	Kagome lattice	12
3	Objectives of this work and strategy	16
4	Methods	18
4.1	Micromagnetic simulations	18
4.2	Electron beam lithography	20
4.2.1	Principle of EBL	20
4.2.2	Sample fabrication and characterization	21
4.3	Magnetic force microscopy	23
4.3.1	Principle of MFM	23
4.3.2	Measurement	24
4.4	Demagnetization protocols	26
4.5	Image processing and analysis	28
4.5.1	Post-processing of measured data	28
4.5.2	MFM image analysis	28
4.5.3	Labview software for MFM analysis	29
4.6	The methodology of the experiment	31
5	Results and discussion	32
5.1	Bringing the dipolar kagome ice in its ground state	32
5.2	Towards the investigation of exotic, cooperative phenomena	35
6	Concluding remarks	42
7	Bibliography	43
8	Acronyms	46

1. Preamble

In 1933 Giauque et al. discovered that frozen water in its hexagonal phase has non-zero entropy [1] even at low temperature. This seems like a violation of the third law of thermodynamics. However, Linus Pauling [2] explained this phenomenon by showing that this intriguing property is caused by the fact that frozen water is frustrated material. The inability of satisfying all interaction at the same time leads to constant movement and flipping of the water molecules. The non-zero entropy is caused by the fact, that the system even though is in solid phase, it locally changes its internal configuration, and therefore, it was more similar to the liquid. Frozen water gave a name to the materials which are used for probing spin frustration. these systems are called *spin ice*.

In this work, we study magnetic interaction in the specially designed lithographically patterned arrays of connected nanoislands. Components of these arrays are geometrically frustrated – that means that due to the geometry of the system, not all magnetic interaction can be satisfied. These so-called *artificial spin ice* (ASI) systems were introduced as a suitable model for studying spin frustration in the matter. Advantages of ASI are that these systems are tunable and it is possible to measure them directly in a real space by using imaging techniques such as *magnetic force microscopy* (MFM).

The focus of this study is kagome lattice [3]. For this special lattice, some exotic behaviour was predicted. In a low energy state of kagome lattice spins are ordered and disordered at the same time [4, 5]. This behaviour is called *fragmentation of the spin*.

Many attempts to reach low energy phases of dipolar kagome spin ice systems have been made [6, 7, 5], but so far nobody was able to probe and measure all phases of kagome system by using MFM.

In this work, we present a way how to reach low energy states of dipolar kagome spin ice system with using lithographically patterned arrays of nanomagnets that we designed.

2. Artificial spin ice systems

Lithographically patterned arrays of nanomagnets can be used to investigate many interesting magnetic properties of matter such as Coloumb phase [8] or fragmentation [4, 5] that would be difficult or impossible to study otherwise. For studying collective behaviour of spins in the matter, *artificial spin ice* ASI systems were introduced [9]. This chapter is dedicated to introduction into problematic of ASI.

2.1. Background

The origin of the ASI is linked with the observation of unusual properties of matter that in the time of discovery seem to violate the laws of thermodynamics. Before exploring the ASI systems, some important background information needs to be discus, such as new exotic phases of matter in section 2.1.1, problems with non zero or even infinity entropy of the system in section 2.1.2 – the origin of such behaviour in section 2.1.3 and link between real nature ASI system.

2.1.1. The three main phases of matter

It has been known that matter can have different phases depending on various parameters such as pressure, temperature, concentration of each component, etc. The schema of the general phase diagram of the matter is shown in Figure 2.1. Depending on pressure and temperature the matter can be in solid (green area), liquid (blue area), gas (pink area) and supercritical fluid phase (grey area). All phases (except supercritical fluid) are separated by phase transition curves: EF curve is sublimation and desublimation and represents phase transition between solid and gas phase. FH curve stands for melting and solidification phase transition between solid and liquid and FG is vaporization and condensation phase transition curve between liquid and gas phase. The F point is called the triple point where all three phases can coexist. If the parameters are changed in a way that pT coordinates are in a different phase than before, we say that the material undergoes a phase transition. From this phase diagram we could assume that the matter should be in the solid phase at low temperature – so for all matter, there should be some phase transition EF and FH curves.

Some theoretical predictions [10] indicate that for special types of systems there is no order even at the low temperature. That means that even at low temperature material remain in liquid disordered phase. This kind of materials does not have phase transition leading to solid phase neither from liquid nor gas. In a liquid phase, there are parameters (atom position, magnetic moment orientation, etc.) that are always fluctuating – even at a thermal equilibrium without external energy. If the material is in the liquid phase even at the lowest possible temperature, it means that such system cannot be frozen and the ground state of this kind of system is many times degenerated. Even without adding additional energy to this system, the system can change its internal configuration [2].

Examples of systems that are disorder-free from a structural point of view, but extensively, magnetically disordered will be discussed in section 2.2. Because of the extensive magnetic degeneracy of such systems, the statistical entropy is non zero and remains finite per site, even at zero temperature. This behaviour contradicts the third law of thermody-

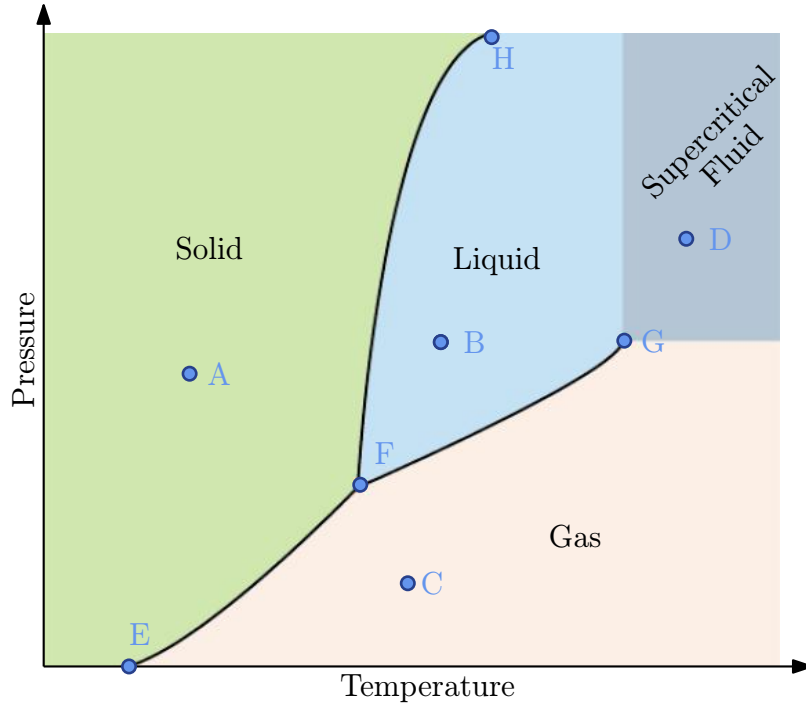


Figure 2.1: General phase diagram of matter showing phase dependence on temperature and pressure.

namics as it was formulated by Max Planck. Planck’s formulation and discussion about third law of thermodynamics is discussed in the following section 2.1.2.

2.1.2. Link with the third law of thermodynamics

Ludwig Boltzmann formulated entropy as:

$$S(N, U) = k_B \ln g(N, U), \quad (2.1)$$

where S is entropy, k_B is Boltzmann constant¹ and function $g(N, U)$ is a degeneration function which describes how many possibilities there are for the system to have required properties such as N number of particles and U internal energy [12].

There are many definitions of the third law of thermodynamics. The most common definition of the third law of thermodynamics was made by Max Planck [13] who stated that: “*When temperature falls to absolute zero, the entropy of any pure crystalline substance tends to a universal constant (which can be taken to be zero).*”

Mathematically speaking:

$$S \rightarrow 0, \text{ as } T \rightarrow 0. \quad (2.2)$$

This formulation of the third law of thermodynamics is valid for most crystalline materials, but it has been shown that some materials have non zero entropy even at the lowest possible temperature.

On the other hand, Albert Einstein formulated the third law of thermodynamics as [13]: “*As the temperature falls to absolute zero, the entropy of any substance remains finite.*”

¹ $k_B = 1.3806504 \cdot 10^{-23} \text{ JK}^{-1}$ [11]

2.1. BACKGROUND

Both of these definitions rely on the presumption that function g goes to the small constant number when the temperature is low. Function g can be dependent on a number of particles in a system as will be shown in section 2.1.3 below. This dependence leads to the fact that entropy of the system is dependent on its size as well. If a system with these dependencies has infinite size, the entropy goes to infinite.

The fact that there are some systems that have puzzling behaviour which seems to contradict Planck and Einstein formulations of the third law of thermodynamics is the reason why it is interesting to study such systems. Although some publications, about non zero entropy at the lowest temperature, were published [14, 15], geometrically frustrated systems still holds many puzzling behaviours that are yet to be explained.

2.1.3. Geometrically frustrated systems

Frustration is the inability of satisfying all interactions at the same time. Geometrical frustration comes from the geometry of the system that does not allow such satisfaction [16]. The best way how to show the behaviour of frustration in the system is comparing frustrated and unfrustrated systems.

Firstly, we will discuss two types of 2D geometry: hexagonal and triangular and two types of interactions:

1. Ferromagnetic (FM) interaction – interactions between first neighbours is minimized when neighbours have the same color.
2. Antiferromagnetic (AM) interaction – interactions between first neighbours is minimized when neighbours have not the same color.

Colour represents some parameter of the lattice component for example spin orientation – orange is spin up, blue is spin down. If the system prefers ferromagnetic (FM) ordering of the system, the result would be as in Figure 2.2 where a) is two possible configurations of hexagon system with FM interactions and b) shows two possible configurations of the triangular system with FM interactions. For both hexagonal and triangular geometry it is possible to satisfy all FM interactions. Therefore, systems in Figure 2.2 are unfrustrated.

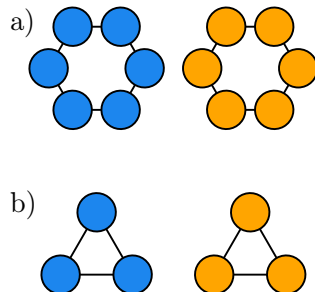


Figure 2.2: Unfrustrated systems: a) Possible configuration of a hexagon with FM interactions. b) Possible configuration of a triangle with FM interactions.

If we change the nature of interaction from FM to AF, systems will want to alternate color of its components. For hexagonal lattice we can see in Figure 2.3 a) that there are two possible ways how to satisfy all interactions in systems. If we add another hexagon into the lattice as it is shown in Figure 2.3 b) there are still only two possibilities how to

satisfy all interactions, and therefore the number of possible ground state is given by the equation

$$g_{\text{hex}} = 2, \quad (2.3)$$

where g_{hex} is the function of degeneration of the states with the lowest energy in a hexagon string.

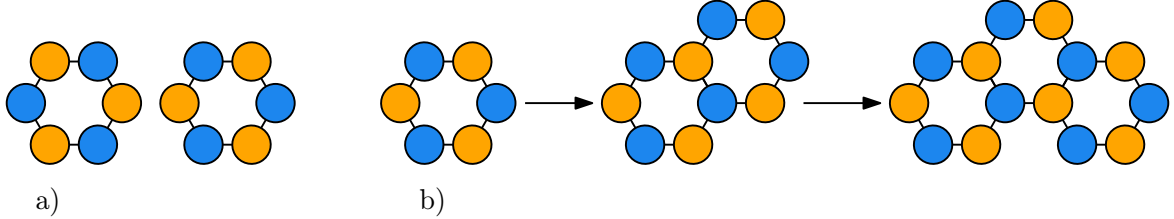


Figure 2.3: Unfrustrated system: a) Possible configuration of a hexagon with AF interactions. b) Possible configurations of a string of hexagons with AF interactions. The number of configurations does not depend on numbers of hexagons in the string, and the configuration is decided by the first hexagon.

The entropy of a system that is shown in Figure 2.3 is independent of the size of the system and follows the third law of thermodynamics formulated by Planck.

AF interaction in triangle leads to frustration. Because of an odd number of particles in the lattice, it is impossible for the system to alternate color for each of its components. This triangle has six possibilities how to be in the energetically lowest possible state. These states are shown in Figure 2.4 a) and for each of them, one interaction is unsatisfied. If we add another triangle to the system, we have three possibilities how to maintain the system in an energetically lowest configuration. Thus, the number of possible configurations g_{tri} (where only one interaction is unsatisfied per triangle) is strongly dependent on the number of triangles n in the system

$$g_{\text{tri}} = 6 \cdot 3^{n-1}, \quad (2.4)$$

where g_{tri} is the function of degeneration for a string of triangles.

In Figure 2.4 b) is shown how the entropy of this kind of system strongly dependent on its size, and it is infinite if the system is infinite.

Comparison of *magnetic force microscopy* (MFM)² measurement of hexagonal and triangular lattices of nanoislands AF interaction is shown In Figure 2.5. We can see that unfrustrated system in Figure 2.5 a) is ordered. On the other hand, MFM signal of the triangular lattice is disordered because of geometrical frustration as can be seen in Figure 2.5 b).

Geometrical frustration in 3D works on the same principle. A good example of 3D geometrically frustrated system is frozen water. In Figure 2.6 a) is shown how molecules of water are ordered in the solid phase in tetrahedra. Due to the different electronegativity of hydrogen and oxygen atoms, partial charges are generated in molecules of water. Electric dipoles generated by partial charges are shown in Figure 2.6 b). The problem is that all electric dipoles are separated by the same distance, and that leads to the impossibility of satisfying all electrostatic interactions as was discovered by Bernal and Fowler [18]. All dipoles can point only towards or outwards to the center of tetrahedra.

²Principle of MFM will be described in section 4.3

2.1. BACKGROUND

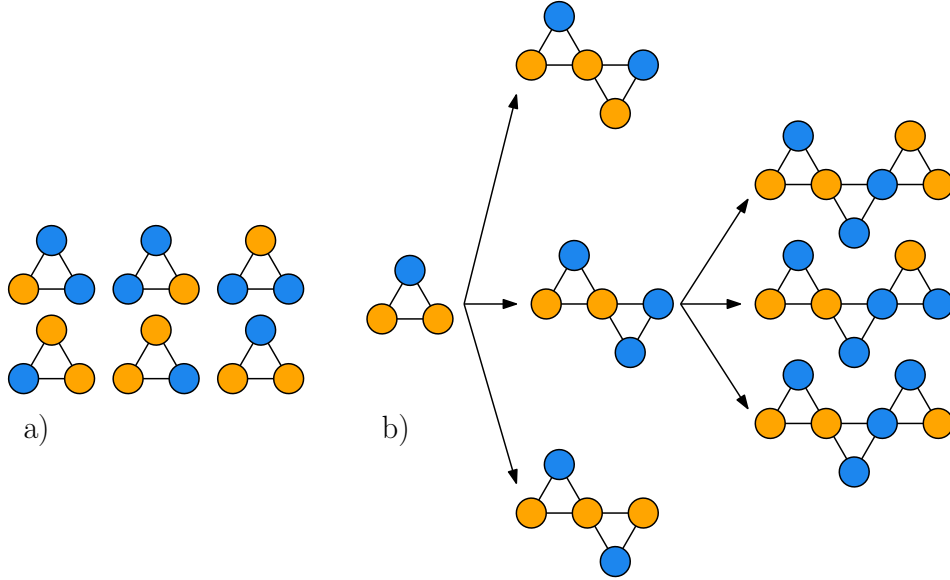


Figure 2.4: Frustrated system: a) Possible configuration of a triangle with AF interactions. All configurations are energetically equal. b) Possible configurations of a string of triangles with AF interactions. The number of configurations strongly depends on the number of triangles in the string.

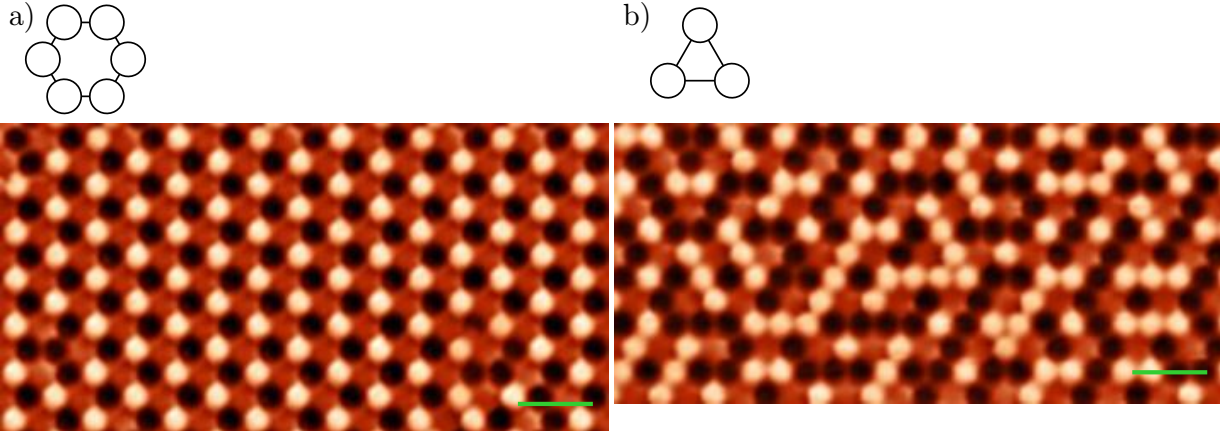


Figure 2.5: MFM images of permalloy nanoislands of a) hexagonal and b) triangular lattice, the green lines in images represent $1 \mu\text{m}$ distance. Images are taken from [17].

For this system is only way how to minimize its energy if each oxygen has two close and two far hydrogen ions – this cause that only two dipoles point towards and two outwards to the center of tetrahedra. This condition is often referred to as two in, two out *ice rule*.

For a given oxygen ion, there are 16 possible configurations of electrostatic dipoles (four dipoles and each can point in two directions: toward and outwards), only 6 of these possibilities obey the ice rules. For N oxygen atoms there are 2^{2N} configuration possibilities [19] if this number is reduced by factor $6/16$ (to acquire a number of possible states with lowest possible energy) we get:

$$g_{water} = 2^{2N} \cdot (6/16)^N = (3/2)^N, \quad (2.5)$$

this leads to non zero entropy which depends strongly on the size of the system.

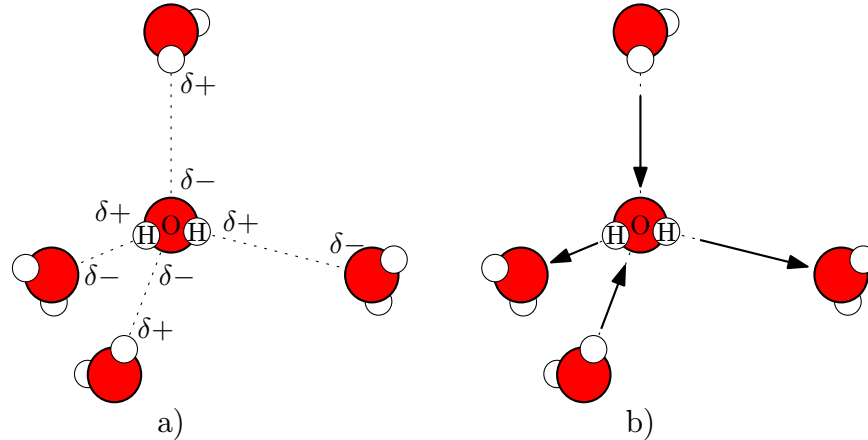


Figure 2.6: a) Schema of molecules of frozen water which are assembled in tetrahedral configuration and their partial charges $\delta+$ and $\delta-$. b) Schema of electric dipoles in frozen water, due to the geometry of the system all electrostatic interactions cannot be satisfied at the same time.

2.1.4. From ice to spin ice

For a few decades now researchers are interested in probing exotic systems that seem to have non zero residual entropy at low temperature due to geometrical frustration. Residual entropy was first observed on frozen water in its hexagonal phase [1]. This puzzling behaviour was explained by Linus Pauling in 1935 [2].

Special pyrochlore crystals were introduced to study properties of matter that are leading to non zero entropy and even more puzzling phenomena. The crystals such as $\text{Dy}_2\text{Ti}_2\text{O}_7$ and $\text{Ho}_2\text{Ti}_2\text{O}_7$ [20] were a great playground for studying geometrical spin frustration. In pyrochlore crystals, interactions between the spins were causing frustration and non zero entropy similarly as in frozen ice, and this fact gave them a name *spin ice* (SI) systems. Measurement of these crystals requires very low temperatures and, moreover, it is impossible to access local information of the materials – all information is averaged across the bulk. Therefore it is impossible to acquire them directly in real space.

In 2005 Wang et al. [9] came up with the idea how to transfer measurement of SI crystals to a 2D problem with specially designed artificial arrays. ASI systems are lithographically made arrays of micro- and nano-magnetic structures. Components of ASI array have to be small enough to be single domain magnets and thus mimic the behaviour of the spin system. These structures allow us to probe exotic properties of matter that would be difficult to study otherwise and most of all we are able to explore the collective behaviour of given system in real space by using imagining techniques such as MFM. Thanks to the real space measurement ASI array can be probed locally and globally at the same time, so local parameters of the system are accessible. Another advantage is that experiments do not have to be conducted at the low temperatures because ASI arrays are athermal³ [19].

³Configuration of the system cannot be changed by thermal energy at room temperature.

2.2. Ising spin lattice models

Since Wang et al. published their work, various types of model lattices were designed and studied [21]. The most probed lattice so far are square lattice and kagome lattice. Both will be described further in the text.

2.2.1. Square lattice

The first attempt to create ASI system by using lithography aimed to mimic the behaviour of spins in pyrochlore crystals. Frustration in such crystal is shown in Figure 2.7 a) where spins are placed in corners of a tetrahedron and point only towards or outwards to the center of the tetrahedron. At low temperature, this kind of crystal follows ice rule. The energy of the interaction between spins is given by exchange energy [22]

$$E_{\text{exch}} = -\frac{1}{2} \sum_{i \neq j} J_{ij} \vec{s}_i \cdot \vec{s}_j, \quad (2.6)$$

where J_{ij} is coupling constant between spins \vec{s}_i and \vec{s}_j – for each pair of spin J_{ij} can have a different value. In case of SI crystals in Figure 2.7 a) $J_1 = J_2 = J_3$ that means that all interactions between first neighbours are equal.

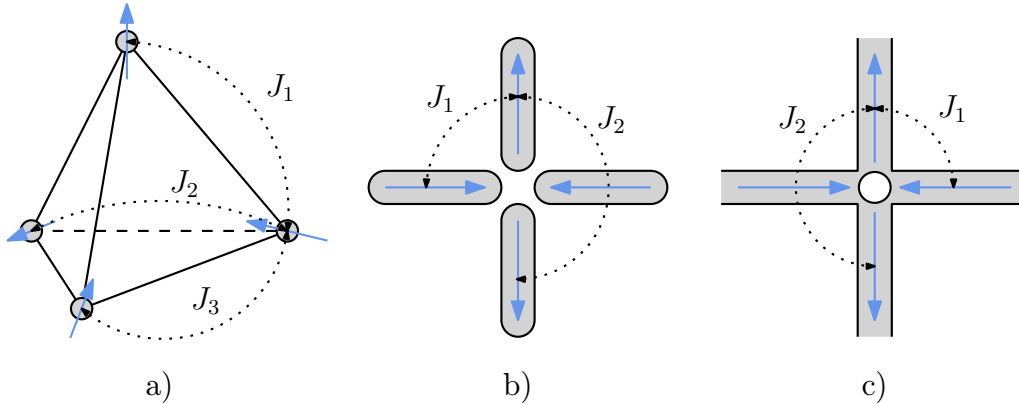


Figure 2.7: Vertices of different type of spin ice system: a) Schema of a spin ice crystal. Interactions between spins are frustrated because of the geometry of the system and exchange constants of interactions $J_1 = J_2 = J_3$. b) Topology and possible magnetic dipole orientation of square lattice. Interactions between the first neighbour are stronger than interaction between second neighbours $J_1 > J_2$. c) Modification of square lattice that more precisely imitates the behaviour of SI crystal because of its coupling constant $J_1 = J_2$.

The artificial lattice that Wang et al. presented is shown in Figure 2.7 b) and it is called square lattice. Components of Wang square lattice are not spins, but magnetic nanoislands. The shape of this nanoisland is crucial. It has to be small enough to be in a single domain state. Each of the islands has only two magnetization states due to magnetic shape anisotropy, which forces magnetic moments to point along the long axis of the islands. This interaction is no longer determined by exchange interactions, but by

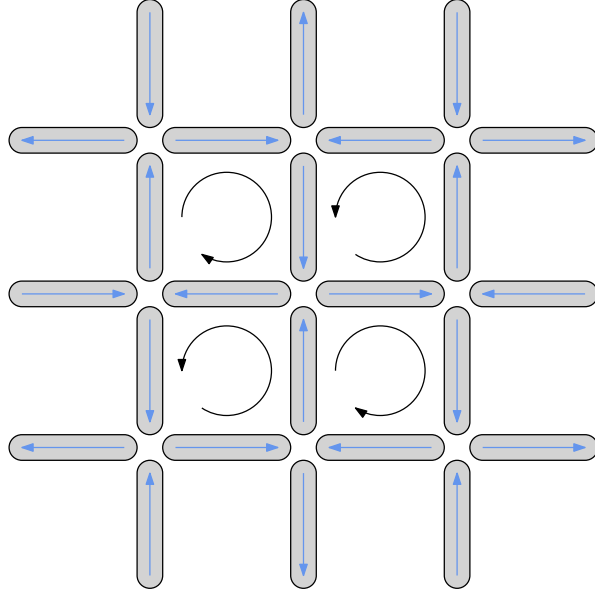


Figure 2.8: Schema of possible ground state of the square lattice. Stronger interaction between perpendicular neighbour forces the system to a configuration where magnetization is oriented in a closed loop.

dipolar interaction. Within the point-dipole approximation,⁴ dipolar energy E_{dip} for two magnetic moments $\mu\vec{S}_i$ and $\mu\vec{S}_j$ located at \vec{r}_i and \vec{r}_j can be calculated as

$$E_{\text{dip}} = -\frac{1}{2} \sum_{i \neq j} J_{ij} \vec{S}_i \cdot \vec{S}_j, \quad (2.7)$$

where \vec{S}_i and \vec{S}_j are normalized spin vectors, and J_{ij} is coupling constant given by equation

$$J_{ij} = -D \left[\frac{1}{|\vec{r}_{ij}|^3} - 3 \frac{(\vec{S}_i \cdot \vec{r}_{ij})(\vec{S}_j \cdot \vec{r}_{ij})}{|\vec{r}_{ij}|^5 \vec{S}_i \cdot \vec{S}_j} \right], \quad (2.8)$$

where $\vec{r}_{ij} = \vec{r}_i - \vec{r}_j$ and $D = \mu_0 \mu^2 / 4\pi$ [23].

From equation (2.8) we can see that coupling constant J can be modulated by changing the spacing parameter in a square lattice between island. It was measured that this system follows ice rule. However, coupling constant $J_1 > J_2$ in case of Wang's square lattice, therefore, if the system is brought down to the ground state, it tends to align magnetic moments in a closed loop manner and satisfy interaction between perpendicular first neighbour as is shown in Figure 2.8.

There have been some successful attempts to modify square lattice in a way that it is $J_1 = J_2$ [24, 25], so it mimics the behaviour of SI crystals more thoroughly. One of this modification is shown in 2.7 c) where islands are connected and have a hole in the middle. Depending on the hole diameter coupling constants change their strength and it is possible to tune the lattice so $J_1 = J_2$.

⁴Magnetic moment of island is held in the center of island with \vec{S} direction and μ power.

2.2. ISING SPIN LATTICE MODELS

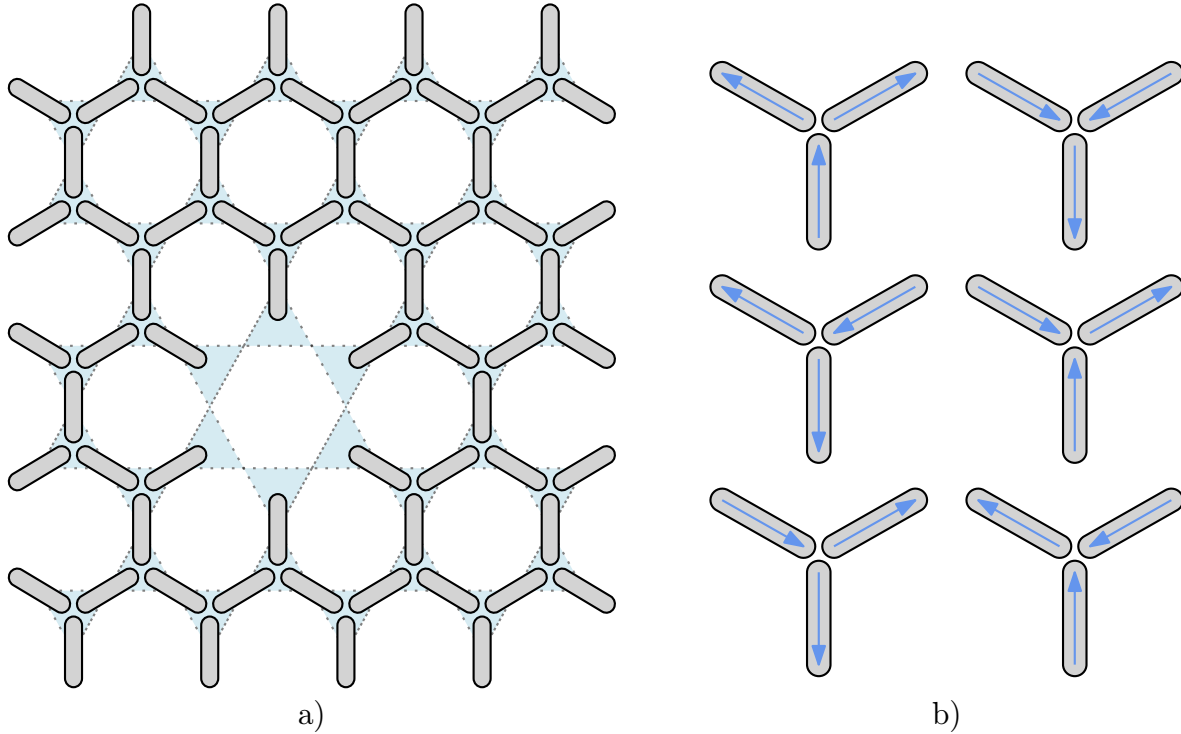


Figure 2.9: a) Schema of kagome lattice. b) Six possible ways how vertex can have the lowest possible energy – representation of ice rule for kagome vertex.

2.2.2. Kagome lattice

Kagome lattice is another geometrically frustrated lattice and was first presented by Saitoh et al. [3] in 2003. It is composed of elongate nanoislands made from magnetic material. Nanoislands are arranged so that each island creates one hexagon side, as it is shown in Figure 2.9 a). As each vertex of kagome lattice is formed by three nanoislands, the configuration is similar to triangle lattice described in section 2.1.3. Because of an odd number of components in vertex – ice rule for kagome lattice is modified to one in, two out (two in, one out) [26] and therefore the ground state of one vertex is six-time degenerated and its configuration can be seen in Figure 2.9 b).

Interactions between macrospins of kagome lattice are dipolar as for the square lattice. So equation 2.7 and 2.8 apply for kagome as well. The main difference is that for the first neighbours all interactions are energetically equal.

Kagome lattice is an excellent example of a system that shows very intriguing behaviour at low energy states. It is predicted that for low energy state kagome lattice exhibit a new state of magnetic matter in which all spins or macrospins are ordered and disordered at the same time [4, 5] this particular behaviour is called *fragmentation*.

Magnetic charge and spin-spin correlations

For a description of kagome lattice, two main parameters need to be defined. First is a *magnetic charge*. The charge of the vertex is defined as the sum of spins which are pointing into the vertex minus spin pointing out of the vertex. Possible magnitude of magnetic charge is: $-3, -1, +1, +3$. If all spins point into (out of) the vertex, the magnetic charge is $+3$ (-3). Vertexes which obey ice rule can only have magnetic charge with a value of $+1$ and -1 for two-in and two-out configuration, respectively.

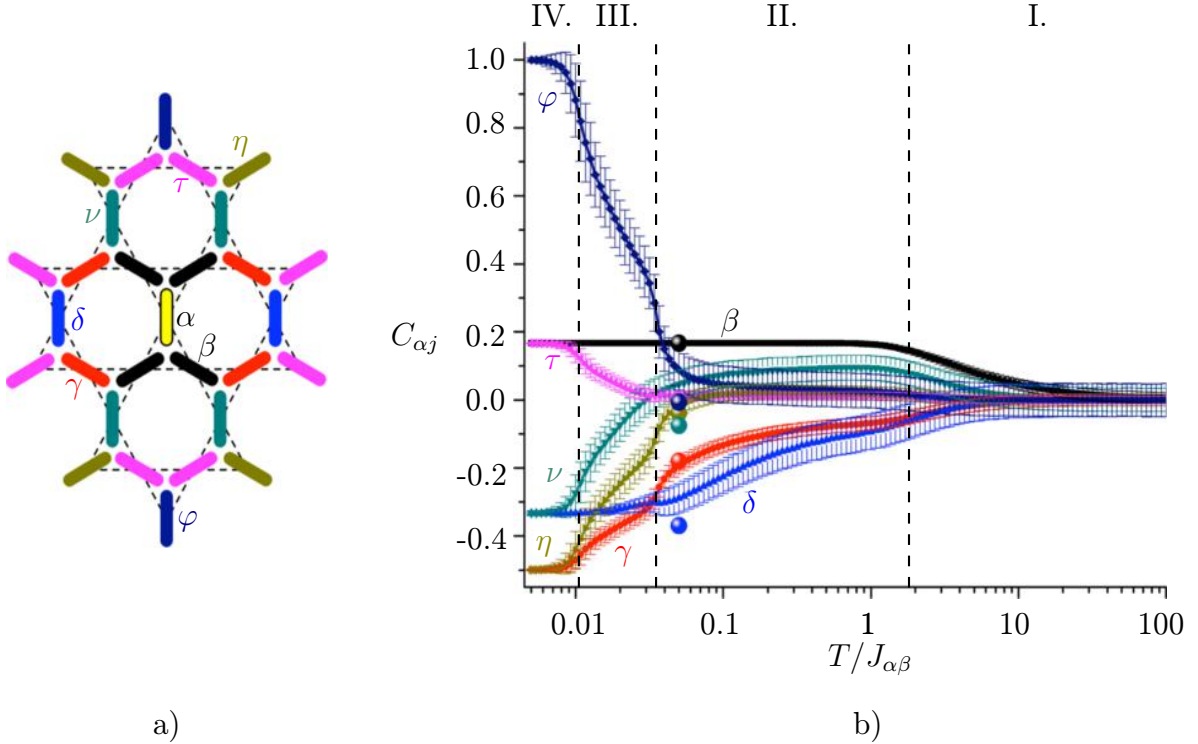


Figure 2.10: a) First seven neighbours of α island: β , γ , δ , ν , τ , η and φ . b) Pairwise spin correlations $C_{\alpha j}$ as a function of temperature T divided by the coupling constant between nearest neighbour $J_{\alpha\beta}$. Regions I-IV. represents four possible phase of kagome lattice: I. Paramagnetic phase, II. Spin ice I., III. Spin ice II. and IV. Long range order phase. Taken and edited from [6].

The second parameter is a *spin-spin correlation*. This parameter tells us how spins in the lattice are correlated. Mean value of correlation coefficients between spins \vec{S}_α and \vec{S}_j are calculated using following equation

$$C_{\alpha j} = \langle \vec{S}_\alpha \cdot \vec{S}_j \rangle. \quad (2.9)$$

First seven neighbours β , γ , δ , ν , τ , η , φ of the island α in kagome lattice are shown in Figure 2.10 a). The spin-spin correlations $C_{\alpha j}$ for the seven first neighbors have been calculated for all temperatures using Monte Carlo simulations⁵ [6] as can be seen in Figure 2.10 b). Each spin correlator has different color and greek letter. The nearest-neighbour coefficients $C_{\alpha\beta}$ are represented in black, while the two nonequivalent third neighbours ($C_{\alpha\nu}$ and $C_{\alpha\delta}$) are shown in green and blue, respectively. The dots correspond to measurement data. Deviations between measured and calculated values for $C_{\alpha\delta}$ and $C_{\alpha\nu}$ are caused by kinetic effects during the magnetization process, that is discussed at [6].

Phases of kagome lattice

To describe phases of kagome lattice, it is advantageous to define normalized temperature as

$$T_n = T/J_{\alpha\beta}, \quad (2.10)$$

⁵The theoretical values for the spin and charge correlations correspond to the average values computed over the set of 10^4 modified Monte Carlo steps used for sampling for each temperature value. Their corresponding standard deviations are also reported in Figure 2.10.

2.2. ISING SPIN LATTICE MODELS

where T is the temperature of the system, and $J_{\alpha\beta}$ is coupling constant between nearest neighbors.

Depending on the normalized temperature of the system, kagome lattice can exhibit one of four different phases [5]:

- I. Paramagnetic phase for T_n larger than ≈ 2 .
- II. Spin ice I. phase for T_n larger than an order of 10^{-1} .
- III. Spin ice II. phase for T_n larger than an order of 10^{-2} .
- IV. Long-range order phase for T_n smaller than an order of 10^{-2} .

Values of spin-spin correlations in the phases I.-IV. are in Figure 2.10 b).

Paramagnetic phase is high energy phase of kagome lattice. Due to the high temperature of the system spins in the system can change its directions. Because all spins are flipping, overall magnetization is zero, and therefore this phase is called paramagnetic. Spin-spin correlations go to zero due to random flipping. Kagome lattice in this phase does not have to obey ice rule, and high energetic configurations with magnetic charge -3 ; $+3$ can be observed.

Spin ice I phase (SI1) is the most common phase of SI. Lattice consist of vertexes which have the lowest possible configuration because all vertexes obey ice rule, and the magnetic charge has value only -1 ; $+1$. There are no long-range interactions between vertexes, and spin-spin correlations are low because system strongly fluctuates but in a way that there is always additional constraint associated with the kagome ice rule.

If the temperature is reduced, system undergoes a first phase transition into the **Spin ice II phase** (SI2). In this phase, another constraint appears. The system still needs to obey ice rule, but in spin ice II phase magnetic charge of the neighbours needs to alternate from -1 to $+1$ this is a condition that leads to the formation of the magnetic crystal [17]. Spins still fluctuate but only if satisfy both of constraints. In this phase, there is the interesting behaviour of the spins. Because of the condition that magnetic crystal – spins needs to be ordered, but on the other hand, spins can fluctuate, and most of the spin-spin correlations do not have large values. Therefore spins has to be somehow ordered and disordered at the same time. This behaviour was the focus of multiple studies in SI [27] and ASI [4, 5].

Long-range order phase (LRO) is a phase that can be referred as the ground state. If the temperature of the system is reduced, even more, the system can undergo another phase transition and long-range order sets in. That means that spins are highly correlated.

ASI systems are an athermal system, and therefore flipping of the macro spins is impossible by temperature. If the temperature is increased magnetic domains, do not flip as spins would but hold still. If the temperature becomes higher than Currie temperature T_C islands become paramagnetic and lose their magnetization. For probing different configurations and phases of ASI system demagnetization protocol are used. This method consists of applying a field demagnetization protocol, i.e., to cycle an external magnetic field in such a way that the overall magnetization of the sample and micro spin orientations are changed by the applied field. The principle of demagnetization protocol will be discussed in section 4.4.

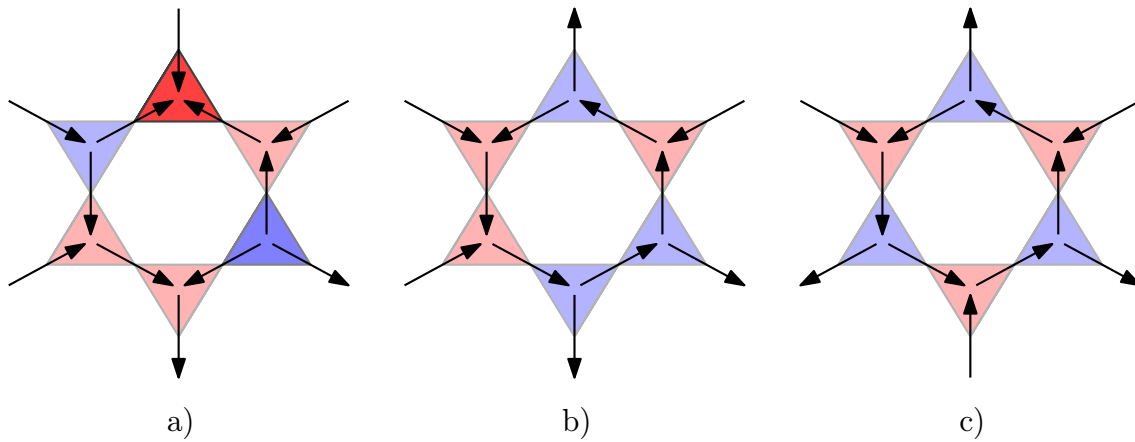


Figure 2.11: Visualisation of possible spin and magnetic charge configuration for a) paramagnetic phase, b) spin ice I phase, c) spin ice II phase. Dark blue triangles and dark red triangles stand for magnetic charge -3 and $+3$ respectively, light blue and light red stand for -1 and $+1$ respectively. Taken from [5].

3. Objectives of this work and strategy

Our goal is to reach and probe exotic low energy phases of kagome lattice that has been described in section 2.2.2.

Anghinolfi et al. [28] provide experimental evidence that this low energy states of the frustrated magnetic metamaterial can be engineered, but they did observed these exotic states in real space measurement. On the other hand, Gartside et al. [29] fabricated kagome lattice and rewrote its spin configuration spin by spin to create a ground state, by using MFM tip. Therefore they were able to observe ground state in real space, but it was done only on small lattice that was made form seven hexagons.

Low energy configurations of kagome lattice are based on the formation of closed spin loops. The loops do not have to be same size or shape, but they must be all over the lattice. In a conventional kagome lattice, it is difficult to reach the state where these loops dominate. Therefore accessing the low energy physic is extremely challenging.

Here in this work, we present a new way how to reach and probe low energy physic of large kagome lattice in the real space. To reach the exotic phases we decided to modify kagome lattice to help loop configuration formed. Firstly, we connect the island, and secondly, we add a notch into the vertex as can be seen in Figure 3.1. By creating the notch we, create some disorder in the lattice.

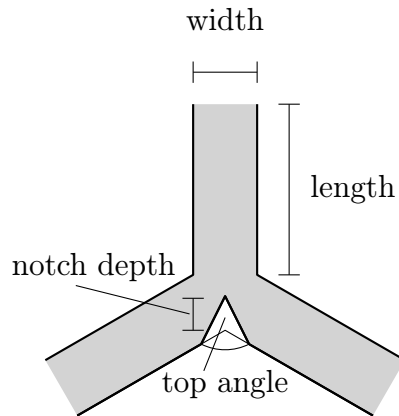


Figure 3.1: Schema of kagome lattice vertex with our modifications. Islands are connected, and into the vertex, a notch has been added.

This notch structure should lift the degeneracy of the lowest possible state. Conventional kagome vertex is six times degenerated as was described in Figure 2.9 b). Our new vertex is only two times degenerated. The magnetic configuration shown in Figure 3.2 in the blue frames has lowest possible energy and both configuration (two in, two out) are energetically equal - this configuration is ground state (GS) of the vertex. Other four configurations (configurations in the red frames) have higher energy and therefore are less probable to occur in the system. The idea is to fabricate sample which is forced by the presence of the notches to be in a state that mimics LRO phase. If we place the notches strategically all across the lattice, we can increase the probability of creating closed lopes of the magnetization. If we are able to obtain a sample in LRO phase, we might force the system to undergo the phase transition into SI2 phase.

3. OBJECTIVES OF THIS WORK AND STRATEGY

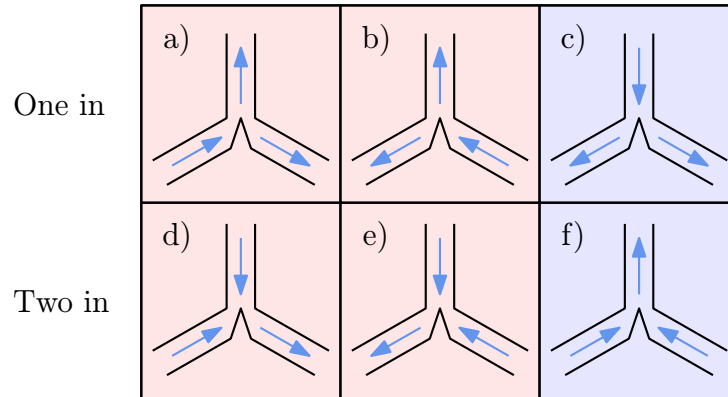


Figure 3.2: Schema of six possible magnetic configurations that obey ice-rule of kagome lattice vertex with the notch. a) b) c) examples show one in ice rule configurations and d) e) f) shows two in ice rule configuration. Total energy $E_a = E_b = E_d = E_e > E_c = E_f$.

4. Methods

In this chapter, all information about sample fabrication and characterization are provided. In the section 4.1, optimization of ASI geometric parameters using modern micromagnetic simulations is shown. Sample fabrication procedure is described in section 4.2 and characterization procedures of ASI systems are described in sections 4.3, 4.4 and 4.5.

4.1. Micromagnetic simulations

We use micromagnetic simulations for estimating the dependence of the vertex energy on its geometry. As a tool for simulations open access software MuMax³ is used [30]. MuMax³ calculates the space- and time-dependent magnetization dynamics in nano- to micro-sized ferromagnets using a finite difference discretization and use *graphical processing unit* (GPU) for some calculations, therefore, calculation time is shorter than calculation time required for simulation with using the only processor.

MuMax³ can also estimate how MFM image of each configuration could look like. Results of the simulation can be seen in Figure 4.1 where magnetic configuration, and MFM images are shown for different notch depth.

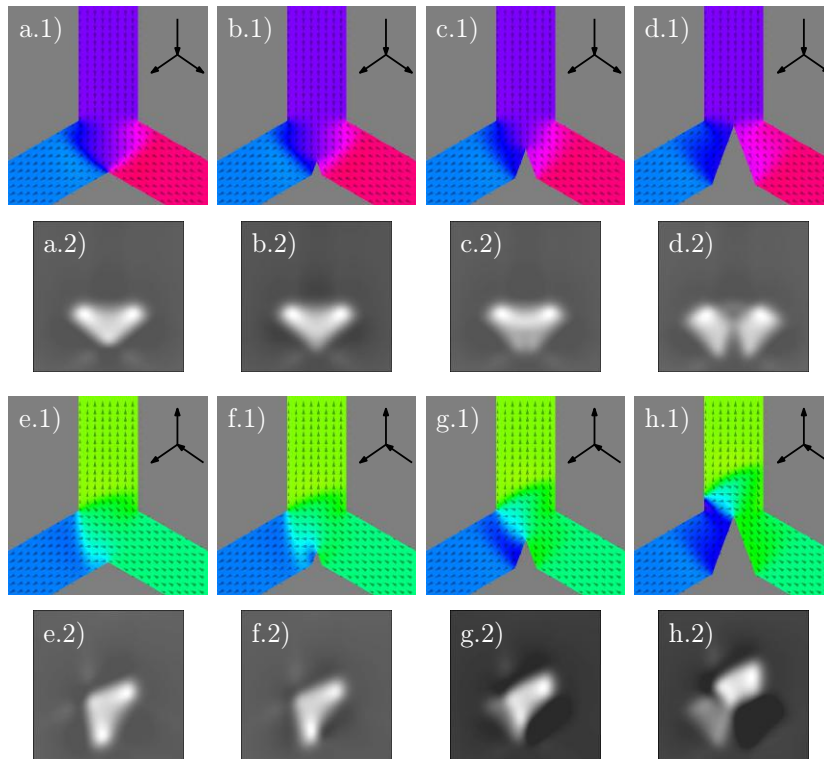


Figure 4.1: Outputs from MuMax³ simulations. Series of images x.1) shows magnetization in vertices and images x.2) shows simulation MFM signal respectively. a), b), c) and d) show ground state configuration for notches with depth: 0 nm, 50 nm, 150 nm and 300 nm. e), f), g) and h) shows higher energy configuration for notches with depth: 0 nm, 50 nm, 150 nm and 300 nm.

Images 4.1 a.1),..., d.1) show ground state magnetization of kagome vertex with notch with depths: 0 nm, 50 nm, 150 nm and 300 nm respectively. Images 4.1 e.1),... , h.1) show higher energy configuration of magnetization of kagome vertex for notch with depths: 0 nm, 50 nm, 150 nm and 300 nm respectively. Images 4.1 a.2),... , h.2) show simulations of the MFM signal of images 4.1 a.1),... , h.1).

The total energy of vertex depends on the depth of the notch and magnetization configuration. Total energy¹ of each vertex was normalized to the energy of the vertex with zero depth of the notch. Results of calculation of normalized total energy for three different magnetization configurations dependence on notch depth are shown in Figure 4.2. Right-sided configuration (RS) is shown in Figure 3.2a), left-sided (LS) is shown in Figure 3.2 b) and ground state (GS) configuration is shown in Figure 3.2 c).

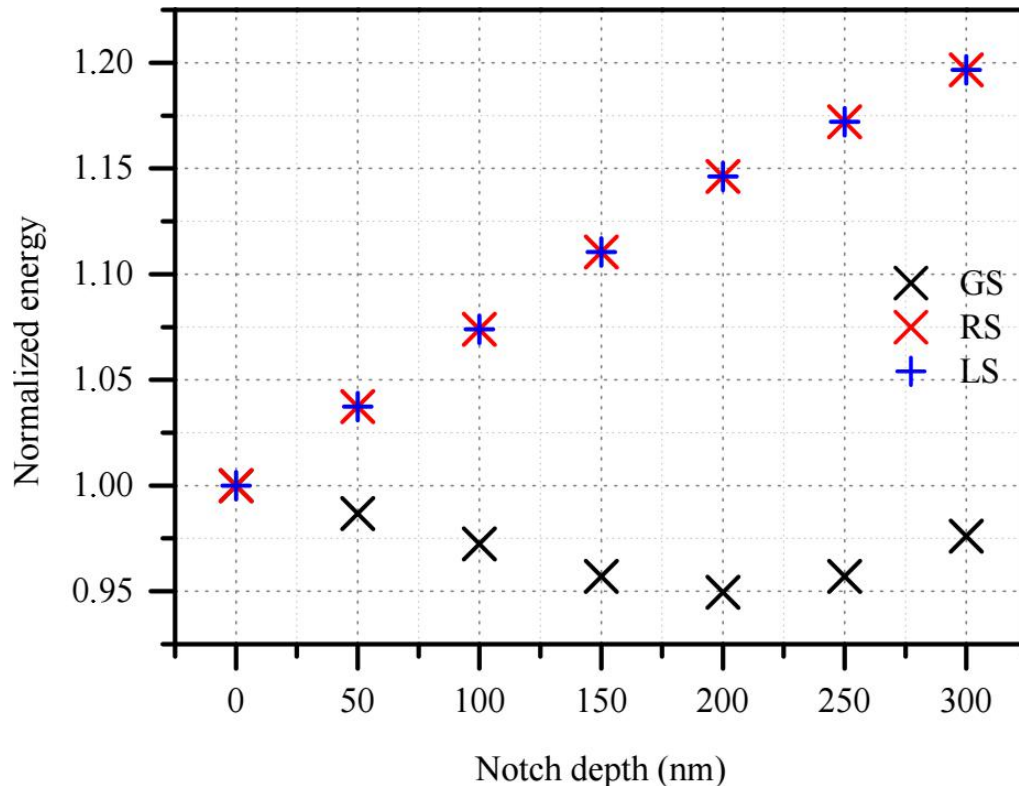


Figure 4.2: The total energy of the vertex for three different magnetization configurations (RS is 3.2a), LS is 3.2 b), GS is 3.2 c)) dependence on notch depth. Energy is normalized to the energy of vertex without notch.

From the simulation, we can see that all configurations GS, RS and LS are energetically equal for vertex without notch (zero depth of the notch). As the depth of the notch increase, the energy difference between GS and LS² arise. This difference means that in lattices GS magnetic configurations with are more likely to occur.

¹Total energy is the sum of exchange energy and demagnetization energy.

²LS and RS configuration have the same energy for each notch, therefore from an energetic point of view LS and RS are the same, and I will only refer to them as to LS.

4.2. Electron beam lithography

Electron beam lithography (EBL) is a technique for preparation micro- and nano- structures.

4.2.1. Principle of EBL

EBL is based on using electron sensitive materials which change its molecular structures after interactions with electrons. These materials are called *resist*. If electron interacts with resist, resist changes its solubility. There are two types of resist: positive and negative. Interaction of electron with positive resist cause degradation of molecular structure, therefore the irradiated area of resist changes in a way that it is more soluble. In case of negative resist electrons on the other hand cause strengthening of bonds in the resist so irradiated area is less soluble.

After exposition³ sample with resist is put into the developer, which is special chemical compatible with given type of resist. Developer removes all area of resist that is more soluble and creates a mask with the design of required nano- or microstructures.

Next major step is to deposit required material onto the sample by any deposition technique such as magnetron sputtering or evaporation. The material covers all surface of the sample, but in the areas where resist was removed by the developer, the material is deposited on the surface of the sample.

The last step of EBL is the removal of the rest of the resist together with all material deposited on it. All major steps are shown graphically in Figure 4.3.

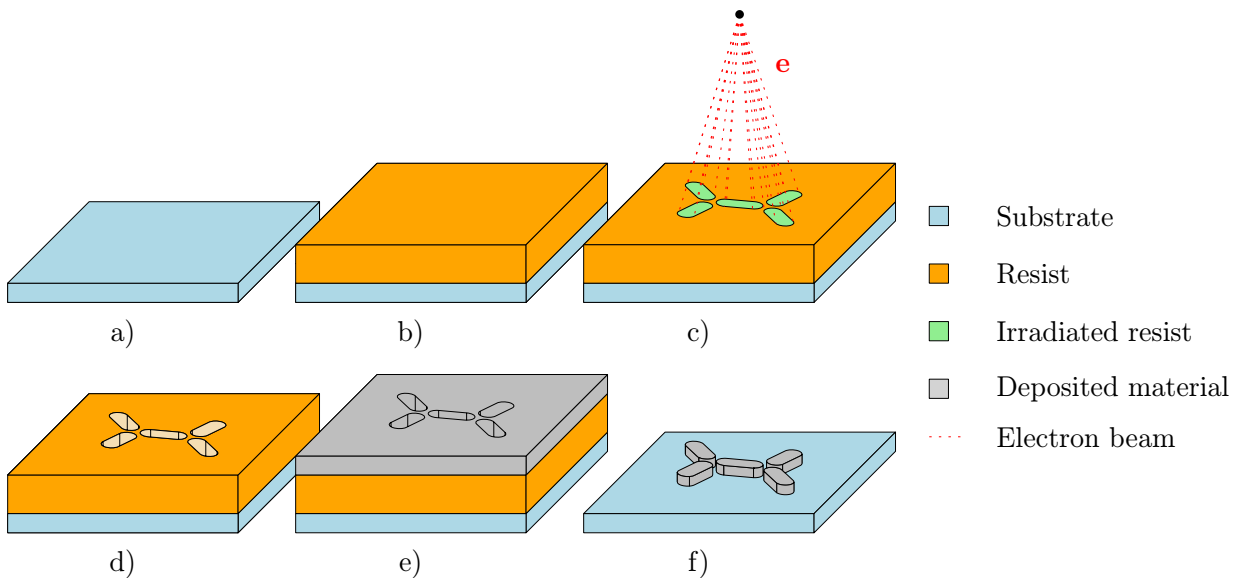


Figure 4.3: Principle of EBL and its major steps: a) Choosing of a suitable substrate. b) A layer of resist is spin-coated on the substrate. c) Exposition of the resist by electron beam lithography. d) Resist after development. The irradiated resist was removed from the sample (in case of positive resist). e) Required material is deposited onto a sample with developed resist. f) Rest of the resist together with all deposited material on it is removed and only desired structures remains.

³Writing with electron beam into the resist.

4.2.2. Sample fabrication and characterization

Fabrication procedure of our NiFe arrays of frustrated vertices is here broken down into individual steps:

1. **Preliminaries** - Silicone substrate was first exposed to ultrasonic bath in acetone for 3 minutes at the room temperature. This procedure helps to clean the surface of the substrate. Secondly, it was exposed to another ultrasonic bath in isopropyl alcohol (IPA) to get rid of the acetone on the surface. After that, the sample was placed on a hot plate for 1 minute at the temperature 150 °C to remove any droplets from the surface.
2. **Spin-coating of resist layer** - Positive resist AR-P 6200.09 was spin coated onto the sample by using spin coater *Lithographic wetbench for coating (SUSS-WETBENCH)*. To achieve a thickness of resist around 50 nm spin-coating speed of the rotation was 6000 rpm with an acceleration 1500 rpm/s for 60 s. After the resist was applied, the sample was again put on the hot plate for 1 minute at the temperature of 150 °C to strengthen the resist.
3. **Resist exposition** - For resist exposition we used lithograph *E-beam writer RAITH 150 two*. The nominal dosage was 100 $\mu\text{C}/\text{cm}^2$ and step size 4 nm with current ≈ 40 pA. Nominal values of nanoisland parameters were length 1 μm ; width 250 nm and depth of the notch 50 nm, 150 nm and 300 nm.
4. **Development of the resist** - To remove exposed resist sample was first immersed into AR 600-546⁴ for 60 s after development sample was risen in demi-water and dried by nitrogen.
5. **NiFe deposition** - Next step was to deposit 25 nm of NiFe layer onto the sample. The deposition was done by using *Electron beam evaporator BESTEC*.
6. **Lift-off** - The last step of sample fabrication procedure is removing the rest of the resist together with all material deposited on it. The sample was put into AR 600-71 chemical for 30 s in order to dissolve unexposed resist. After this step, only material, which was deposited through the resist mask directly on the surface, remains.

After we fabricated the sample, we used *Scanning Electron Microscope* FEI Verios 460L (SEM) for imaging measurement of the sample structures. The overall image of arrays with the depth of the notch 50 nm, 150 nm and 300 nm with zoom in one hexagon of the lattice can be seen Figure 4.2.

⁴A developer is compatible with resist AR-P 6200.09.

4.2. ELECTRON BEAM LITHOGRAPHY

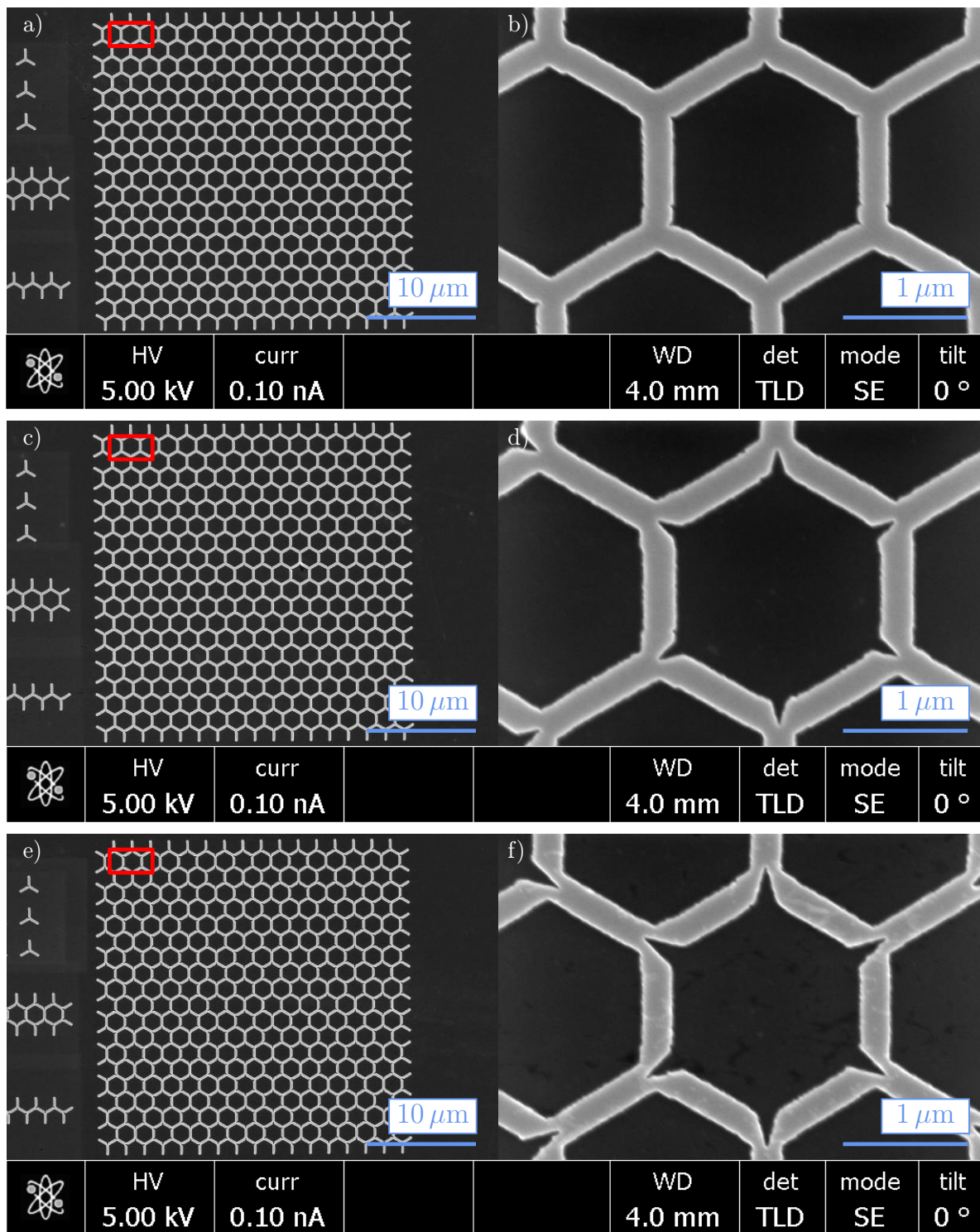


Figure 4.4: SEM images of kagome lattice with notches. Images a), c) and e) show the overall structure of lattices with 50 nm, 150 nm and 300 nm notch depth. Red frames in images a), c) and e) indicate which area is zoomed in pictures b), d) and f) respectively.

4.3. Magnetic force microscopy

MFM is one of the *scanning probe measurement* (SPM) techniques based on the local property measurement of the sample, performed thanks to a specially designed probe. The probe scans each spot in a two-dimensional fashion to construct an image.

4.3.1. Principle of MFM

MFM is a technique which measures the interaction between the probe and stray field emanating from the sample. Detection of the stray field of the sample allows us to derive the distribution of magnetization inside the sample. MFM is a two-pass method based on *atomic force microscopy* (AFM). Both AFM and MFM probe forces between the sample and the sharp tip of the probe. Probe for MFM can be standard nonmagnetic cantilever with a sharp tip coated with a few tens of nanometres of magnetic material. Both AFM and MFM are well-known techniques, and many reviews were written about them such as [31] for AFM and [32]. Here only a basic concept will be described.

During the measurement, the probe does line scans across the sample. Each line is scanned forward and backward in each pass.

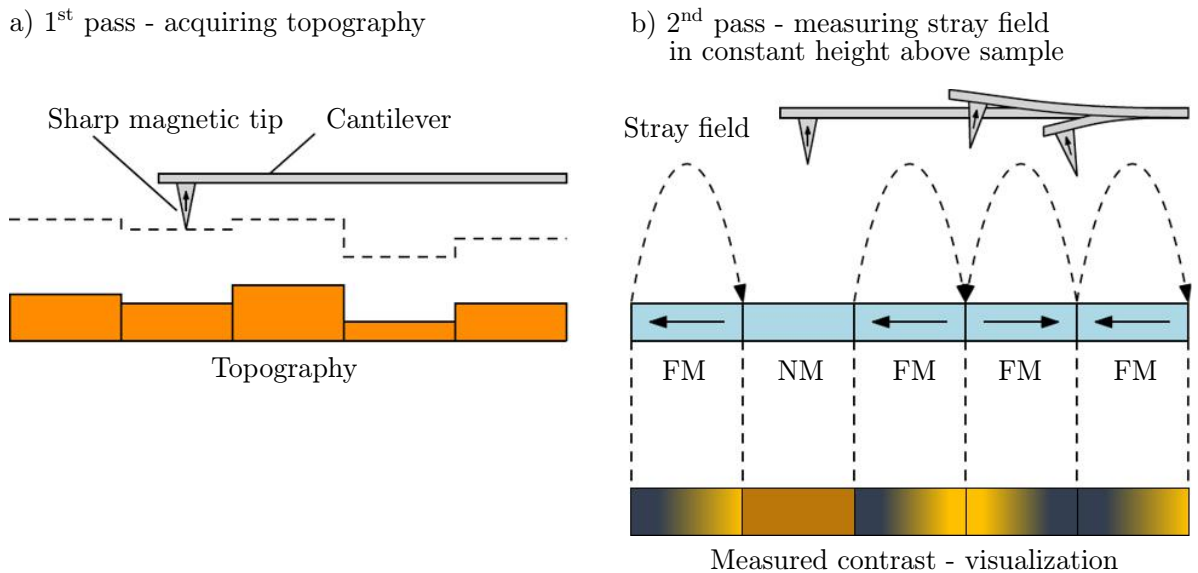


Figure 4.5: Schema of two pass measurement of MFM. a) Acquiring the topography by using standard AFM. b) Schema of interaction between the magnetic tip and stray field of ferromagnetic (FM) domains in a constant height above the sample. The stray field causes a phase shift of the oscillating cantilever. The measured phase shift is in fact visualization of the magnetization of the sample.

The first pass is used for topography detection, and schema of AFM measurement is in Figure 4.5 a). The sharp tip is close to the surface where the van der Waals forces between the tip and the surface dominate [33]. In second pass tip is lifted higher above the sample where magnetic interactions are stronger than the van der Waals forces [33], and then the tip is kept in constant height⁵ above the sample to measure the interaction between the stray field and magnetic tip. In the second pass, cantilever oscillates, and magnetic

⁵Cantilever copy trajectory that was acquired in the first pass.

4.3. MAGNETIC FORCE MICROSCOPY

forces that act on the tip and cantilever change the phase of this oscillations. This phase shift visualizes magnetization of the ferromagnetic domain in the sample. Schema of the second pass of MFM measurement can be seen in Figure 4.5 b) where the magnetic tip is oscillating in constant height above the sample and interacting with the stray field of ferromagnetic (FM) domains. The result of this measurement is phase shift contrast from which magnetization can be determined.

4.3.2. Measurement

For measurement of MFM *Scanning Probe Microscope Bruker Dimension Icon* (ICON) has been used.

For acquiring the topography during the first pass, AFM tapping mode was used. In this mode, a probe is mechanically forced to oscillate on a frequency near its resonance frequency by a piezoelectric crystal. Operator chose amplitude with which the probe oscillates. A feedback loop controls the difference between amplitude setpoint and real amplitude of the oscillation and tries to minimize the difference by approaching or retracting closer to the surface. The outcome of this feedback loop is then a voltage applied to the piezocrystal from which the topography can be estimated. For more information see [34].

After scanning of the topography, probe was lifted higher above the sample. This so-called *lift scan height* was always in range of 40 nm to 90 nm, and it is kept constant during the whole scan. If the lift scan height is the small better lateral resolution is observed.

The typical outcome of MFM measurement can be seen in Figure 4.6 where topography of the fabricated array with a notch depth of 150 nm is shown in case of a) and magnetic contrast of the sample is shown in case of b) where the contrast is similar to the simulated contrast of the vertex shown in Figure 4.1. From magnetic contrast, we can acquire macro-spin orientation and calculate spin-spin correlations, but this process will be discussed in section 4.5.

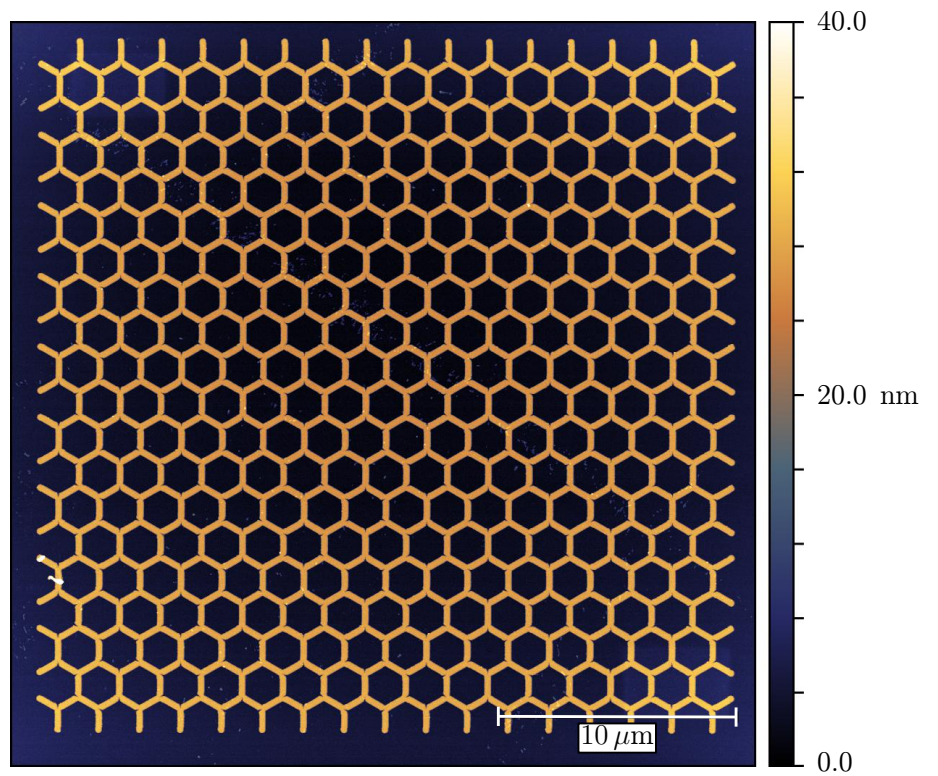
Two types of probes were used:

1. Commercial probes MESP-V2 from Bruker company with Co-Cr magnetic coating. These tips have tip radius around 35 nm.
2. AFM tips AC240TS-R3 from Olympus company that were coated at CEITEC Brno in Electron beam evaporator with 25 nm⁶ of Co material.

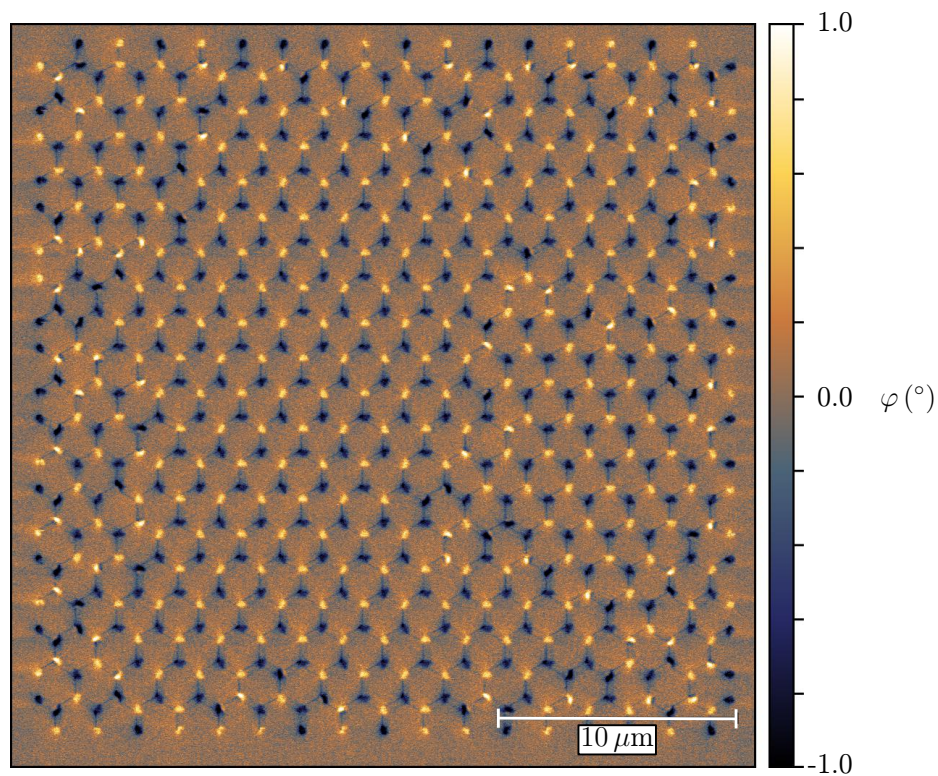
Both of these types of probes acquire really good magnetic contrast, but our “homemade” tips had a better lateral resolution. Comparison of the measurement with MESP-V2 and AC240TS-R3 with coating can be seen in Figure 4.7.

For most of the measurement probes, AC240TS-R3 with “homemade” coating were used.

⁶25 nm was the nominal thickness that was deposited. However, the thickness of magnetic material on the probe apex was smaller.



a)



b)

Figure 4.6: a) Topography of NiFe kagome array with notches of 150 nm depth. The thickness of the array is around 25 nm. b) The magnetic contrast of the kagome array. Contrast of the vertices is similar to the predicted contrast from the simulations.

4.4. DEMAGNETIZATION PROTOCOLS

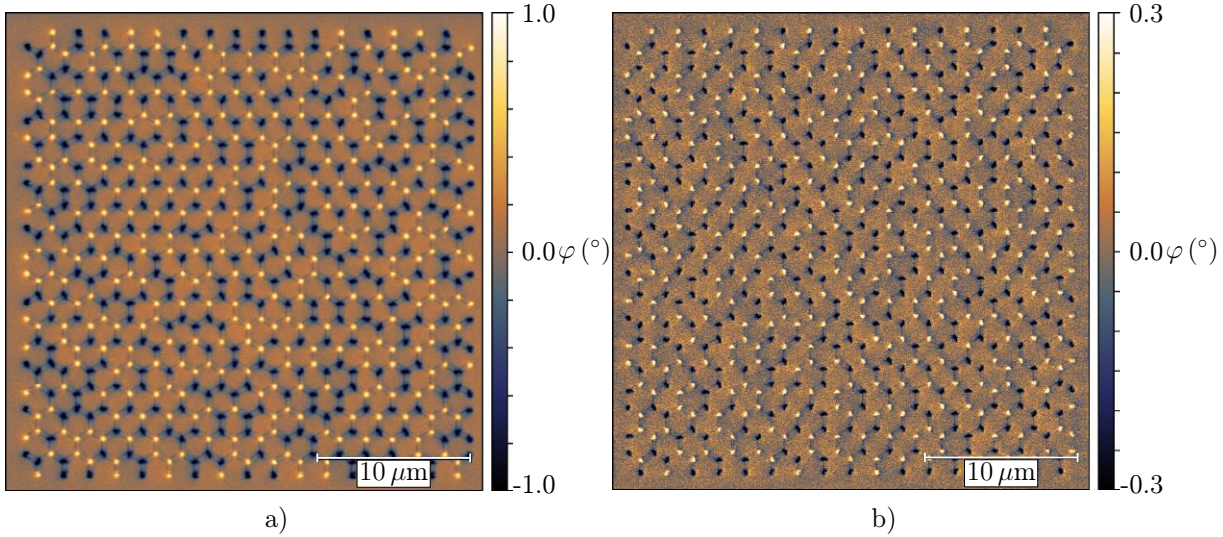


Figure 4.7: Comparison of the measured magnetic contrast with a) MESP-V2 tip and b) AC240TS-R3 with “home made” coating. In case of MESP-V2 signal to noise ratio is much better, but the lateral resolution is worst than in case of “home made” AC240TS-R3.

4.4. Demagnetization protocols

There are many types of demagnetization protocol for example protocols to bring the system to the low energy state [35, 36] of high energy state [37]. For our experiments, we use demagnetization protocol which is shown in Figure 4.8. The sample rotates inside of the in-plane applied external magnetic field. The external field has a sinusoidal shape, and its frequency is much lower than the frequency of sample rotation. This cause that the sample is exposed to almost the same external field from each side. The amplitude of external field decays linearly. If the external field is higher than some effective value B_1 magnetic domains in nanoisland are always forced to be oriented in the orientation of the external field. If the external field is lower than value B_2 , then nanoislands no longer change their domain orientations. Effective demagnetization occurs only in between the field value B_1 and B_2 and it last for time $t_{\text{eff}} = t_2 - t_1$. During the effective demagnetization nanoisland only change its domain orientation if it would result in lowering the total energy of the system. Therefore the longer is the t_{eff} , the lower is the total energy of the lattice. Effective time of demagnetization can be control by either initiate value of the external field B_0 or by the total time of demagnetization t_{dem} . We always set $B_0 = 120$ mT which is a value that can saturate the sample that means above value B_1 . Our demagnetization protocol is control only by the different length of t_{dem} . So if we want the lattice to be in high energy state, we choose short t_{dem} , and if we want to reach low energy state of the lattice, we need to use demagnetization protocol with long t_{dem} .

Experimental set-up of demagnetization can be seen in Figure 4.9. The sample is glued to the fan which provides sample rotation during the demagnetization. The angular frequency of the fan is around 2400 rad/s. This holder is then placed in the gap of the electromagnet that provides external magnetic field. Maximal external field of our electromagnet is 180 mT. Demagnetization protocol is generated from keysight waveform generator. The frequency of the sinusoidal waveform of the demagnetization protocol was 1.6 rad/s.

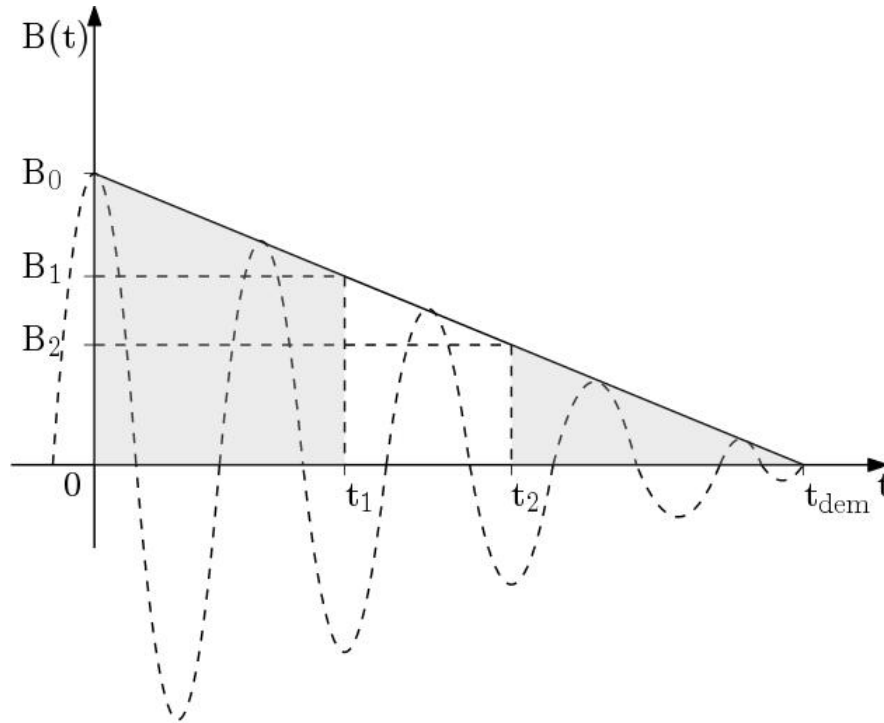


Figure 4.8: Schema of demagnetization protocol. Sinusoidal field with amplitude B_0 that linearly decay for time t_{dem} . Demagnetization of the sample is effective only within a time interval $(t_1; t_2)$.

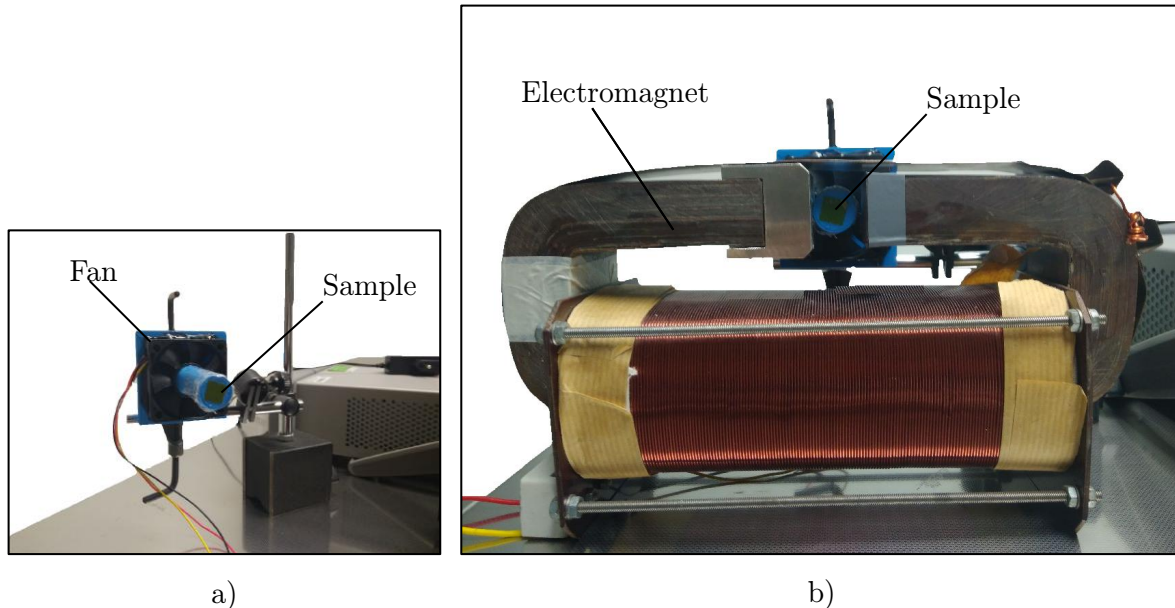


Figure 4.9: Simple demagnetization set up which allow sample rotation within the external magnetic field: a) Sample holder glued on the fan. b) Sample holder placed into electromagnet gap.

4.5. Image processing and analysis

4.5.1. Post-processing of measured data

Post-processing of the measured images is done in open source software Gwyddion. Gwyddion is software for visualization and analysis of SPM data. Basically, only data operation that has been done on AFM image is a correction of constant inclination and correction of the distortions due to scanner imperfection [34].

On the other hand, the purpose of the MFM image was only to give us qualitative information about macrospin orientation. Therefore even non-physical post-processing such as subtracting polynomial background of 11th degree was done.

4.5.2. MFM image analysis

To determine the phase of measured kagome lattice, we need to extract macrospin configuration from MFM signal. Our convention is that bright MFM signal represents the head of the macrospin and dark MFM signal is the tail of macrospin. This convention is the same that is used in MuMax³ simulations. MFM image of lattice consisting of two hexagons is schematically shown in Figure 4.10. Blue and orange shapes simulate dark and bright MFM contrast, respectively. Blue shapes represent vertices with a magnetic charge of -1 , whereas orange shapes represent magnetic charge of $+1$. From the shape of MFM contrast, the spin orientation can be determined – arrows in Figure 4.10 represents spin orientation (red is spin up and blue is spin down). To analyse spin-spin correlations, we are using a program developed by researchers at Néel Institute. The input to this program is the orientation of each spin: $+$ is orientation up and $-$ is orientation down. The spins must be placed into the software in special order that is shown in Figure 4.10 by the numbers next to the spin. Input for this type of simple lattice is therefore: $- + + - + - + - - - + + - - + + - - +$.

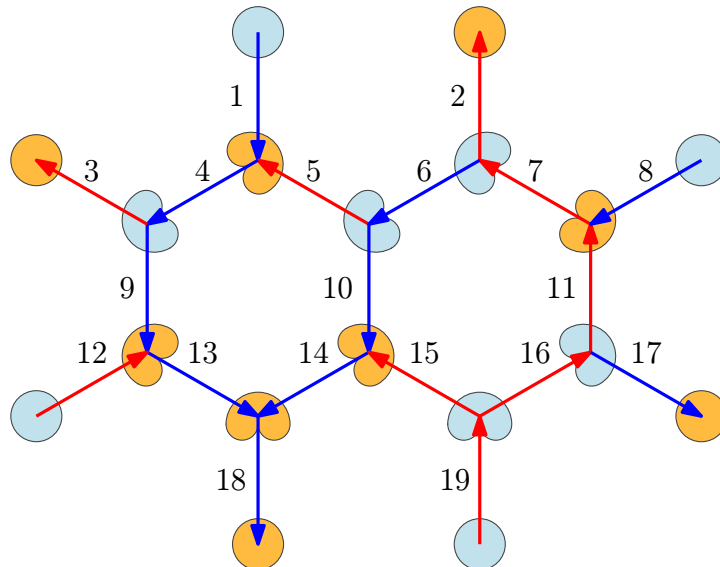


Figure 4.10: Schema of small kagome lattice. Blue and orange shapes represent MFM signal used to determine spin orientations (red and blue arrows). Numbers next to the spins show the order of spin orientations, which is the input of the software for spin-spin correlations coefficients.

The output of this software gives us calculated spin-spin correlation coefficients. For Figure 4.10 calculated coefficients are presented in Table 4.1.

Correlation coefficients $C_{\alpha j}$						
β	γ	δ	ν	τ	η	φ
0.1667	-0.1364	-0.2500	0.0909	0.0000	-0.0714	0.3333

Table 4.1: Correlation coefficients calculated for a lattice in Figure 4.10.

Analysis of as small lattice as is shown in Figure 4.10 is simple task if the resolution of MFM image is good enough. For acquiring a reasonable statistic much larger lattice is required. Our experimental lattices were made of 16x18 hexagons, that means 627 vertexes and 976 spins. Analysis of such large lattice is time consuming⁷ if it is done manually. Therefore, I developed software for automation of the MFM image analysis described in next section 4.5.3.

4.5.3. Labview software for MFM analysis

To make analysis process faster and more user-friendly *Image automatic analysis software* (IAAS) was developed using *LabVIEW* environment. Developing and optimizing of IAAS were a time-consuming process, but in a larger time period, it was worth it because IAAS can be used not only for the purpose of this thesis but even in further research of spin ice systems. LabVIEW was chosen as programming platform as it has various modules for identifying and comparing objects in the image⁸, and design of user interface is relatively simple.

IAAS user interface is shown in Figure 4.11. Image analysis using IAAS is done in following steps:

1. **Loading images** – AFM and MFM images are loaded into IAAS.
2. **Marking vertices of AFM image** – User marks the position of first two vertices in a first and second row in AFM image. IAAS completes positions of other vertices in the lattice according to user-defined lattice parameters. The position of each vertex is displayed on top of topography in the panel marked by brown frame in Figure 4.11. The panel marked by blue frame in the user interface allows the user to adjust parameters of the lattice in order to improve positioning of the vertices.
3. **Marking vertices of MFM image** – IAAS transfers positions of vertices to MFM image. Positions of the vertices are shown on top of MFM signal in the panel marked by brown frame in Figure 4.11.
4. **Identifying the spin orientation** – For each vertex, IAAS crops area around the vertex position in MFM image. This cropped image is compared to the database of possible vertex configuration. After the cropped MFM image is recognised as one of the configuration in database, its spin configuration is saved into a matrix.
5. **Ordering the spins** – After all MFM vertices are recognized, software reorder matrix with spin configurations into the order required for spin-spin correlation software.

⁷Manually analysis of our lattice require at least 80 minutes.

⁸In IAAS the NI Vision Development Module is used.

4.5. IMAGE PROCESSING AND ANALYSIS

6. **Setup of spin-spin correlation software** – User can set up parameters (geometry of the lattice, etc.) for spin-spin correlation software directly in IAAS (panel in the violet frame in Figure 4.11) and then launch it.
7. **Vizualisation of spin orientation** – IAAS can run *Mathematica* script that creates a PNG image of spin and charge configuration in the lattice. This step is optional, however, is useful to check correctness of analysis.

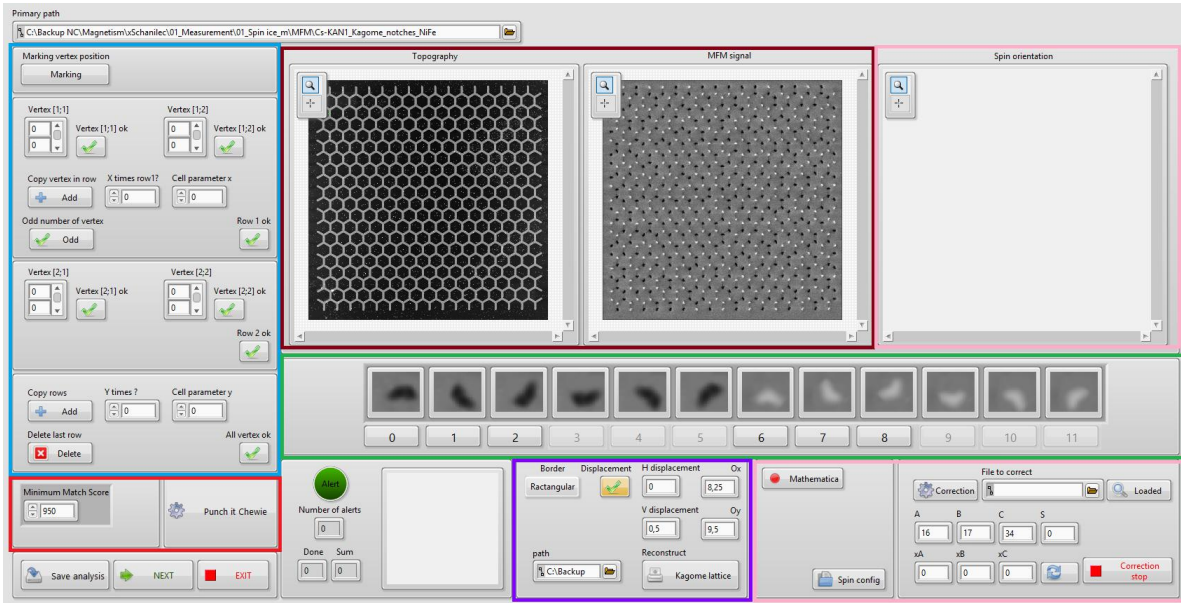


Figure 4.11: The user interface of IAAS. Brown frame marks are where AFM and MFM image of lattice for analysis is shown. Green frame shows a database of possible MFM contrasts. Red frame is automatic analysis toolbox. Blue frame marks the vertices location controller. Violet frame is a panel for communication with spin-spin correlation software, and pink frames show panels for error correction.

The core of the automatic analysis is identifying the configuration of the spin from the MFM image. This process can be conducted by IAAS itself or by the user. Comparison of both options, their advantages and disadvantages, is given in following paragraphs.

First, IAAS automatic recognition of MFM signal with optimized procedure takes about 5 seconds for the lattice of 627 vertices. However, the total time needed for whole analysis depends strongly on the mistake rate of automatic recognition procedure. To avoid mistakes in automatic analysis, very good quality of MFM image is required. For MFM images presented in this thesis, at least 15 mistakes occur during analysis of one lattice. Finding and correcting the mistake is time-consuming procedure – correction of one mistake in automatic recognition can take up to two minutes. Therefore, the total time required for analysis of MFM image with average quality is 40 minutes. The main advantage of IAAS automatic recognition is the speed. However, to exploit this advantage, resolution of the MFM image needs to be as perfect as possible. Otherwise, the mistake rate of the analysis is higher than when the analysis is done by the experienced user. Nonetheless, the complete analysis of average quality MFM image is still faster than manual analysis without IAAS.

The second possibility is user-recognition of MFM contrast. In this case, recognition of MFM contrast is done by the user for the minimum number of the vertices⁹ that are required for covering all spins in the lattice (this number is slightly bigger than half of the vertices – in case of our lattice it is 348). For each analysed vertex, the user is asked to choose the spin configuration from the database, which corresponds best to the MFM signal of the cropped image. A skilled user can analyse average quality image without any mistake within 15 minutes. The advantage of user-detection is precision, which leads to a fast analysis of the lattice. The disadvantage is that analysis requires manpower.

To sum up, user-recognition is better and often faster way how to analyse the image than IAAS automatic recognition. But both of these possibilities are faster, more comfortable than manual analysis without using IAAS. There are several improvements of IAAS, which would make this tool more efficient and versatile, such as: implementing different geometry, upgrade of the auto-detection system with neuron network and implementation of the tool for automatic correction of mistakes. These improvements are planned for next research.

IAAS is attached to this work as supplementary material.

4.6. The methodology of the experiment

Methods described in previous sections are utilized in our experiment in the following way. First, the geometry of the studied lattice is designed using micromagnetic simulations. Samples with chosen geometry are fabricated using EBL. The spin configuration of each sample is studied for different energy states, which are achieved by applying different demagnetization protocols – total time of demagnetization varies from one week to half a second. Demagnetized samples were measured by MFM, and spin configuration was analysed using IAAS (developed as a part of this thesis) and spin-spin correlation software (developed at Néel Institute).

⁹all vertices at the edges of the lattice and every second in the bulk of the lattice

5. Results and discussion

In this chapter, we present results of measurement of kagome lattices with different depth of the notch after applying various types of demagnetization protocol. We were able to observe ground state (LRO phase) as can be seen in section 5.1. In section 5.2 we show that our system can reach SI1 phase and even phase that is at the border between SI1 and SI2 phases. On the last mentioned phase, we were able to prove the existence of exotic collective phenomena – fragmentation.

5.1. Bringing the dipolar kagome ice in its ground state

As was mentioned before in chapter 3, we want to reach to the low energy state of kagome lattice by applying the new strategy. So far the attempts to reach low energy states was made by creating a lattice that is in SI1 phase and try to force the system to undergo the phase transition to SI2 and possibly LRO phases. We would like to reach and observe ground state configuration in real space on large lattices – that is something which has not been done before.

Our strategy is to fabricate a lattice that would prefer to be in LRO (ground state) phase and excite this lattice to undergo a phase transition into SI2 phase.

The first step of our strategy is to find parameters of both lattice and demagnetization protocol, so that lattice reach ground state.

First we demagnetize the sample for a week, and we were not able to observe large patches of ground state configuration in lattices where the notch depth was 50 nm and 300 nm. However, we discovered that lattices with notch depth 300 nm are not suitable for our experiment due to the occurrence of magnetic defects which are visible in Figure 5.1 b).

Defects only appear in nanoisland with two notches within. It seems that defect in a red circle is caused by out-of-plane magnetization or by the existence of some complicated in-plane domain. The defect in white circle is simply extra domain wall that was formed to minimize the energy of two macrospins pointing into the center of the island. On the other hand, nature of these defects is interesting, and they might be useful in a future as a tool for bringing disorder and excitation to the lattice.

Although we can see some patches of the ground state in the Figure 5.1 they are not as perfect as in lattices with the depth of the notch 150 nm that are shown in Figure 5.2. These lattices reach almost perfect ground state after one week demagnetization.

The almost perfect ground state was observed on various lattices with the depth of the notch 150 nm after seven days demagnetization process. In Figure 5.2 AFM and MFM signal of three different lattices. Especially for images 5.2 d) and f) defect in ground state structures are only at the edges. This behaviour is caused by the fact that the vertices at the edges do not have neighbours. Therefore some magnetic “surface” relaxation occurs.

From MFM signal that is shown in Figure 5.2 d) spin-spin correlations were calculated. Firstly we used all vertices for this calculation and the values the correlation coefficient of

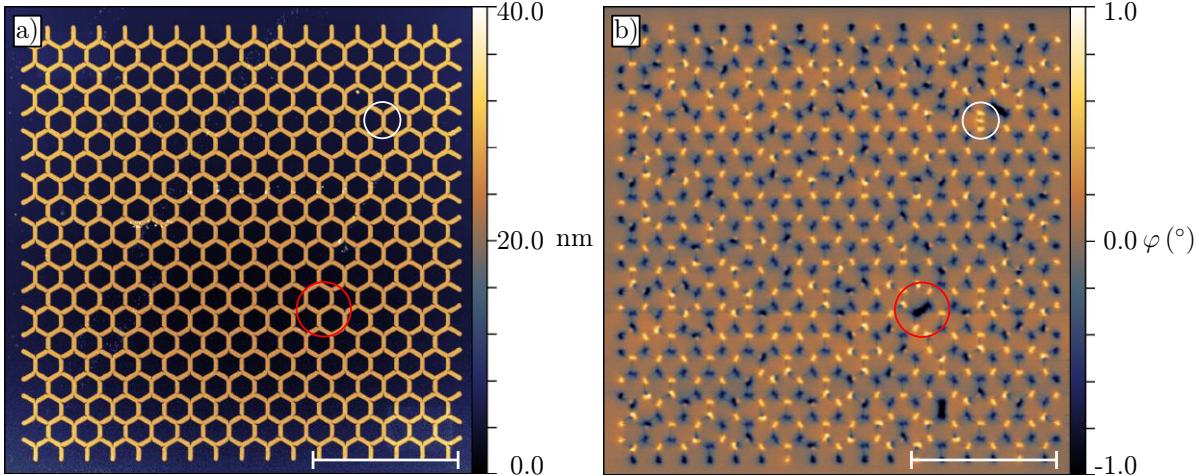


Figure 5.1: Lattice with the depth of the notch 300 nm after seven days demagnetization. a) The topography of the measured lattice with notch depth 300 nm. b) MFM signal corresponding to the lattice shown in the image a). Red and white circles show where magnetic defects are. In the red circle, it would seem that magnetization of the whole island is out-of-plane or that some complicated in-plane domains are presented. In the white circle, it seems that extra domain wall in the nanoisland was formed to minimize the energy. Both of these types of defect occurs only in nanoisland that has two notches within. White lines in the images represent the distance of 10 μm .

first seven neighbour are shown in Table 5.1. Then we calculated the effective temperature of the system as a minimum of a spread-out function

$$K(T/J_{\alpha\beta}) = \sqrt{\sum [C_{\alpha j}^{\text{exp}} - C_{\alpha j}^{\text{MC}}(T/J_{\alpha\beta})]^2}, \quad (5.1)$$

where $C_{\alpha j}^{\text{exp}}$ are correlation coefficients from experiment and $C_{\alpha j}^{\text{MC}}$ are correlation coefficients from Monte Carlo simulations taken from [7]. The effective temperature of the system is shown in Table 5.1 as well.

Correlation coefficients $C_{\alpha j}$							Effective temperature $T/J_{\alpha\beta}$ (a.u.)
β	γ	δ	ν	τ	η	φ	
0.167	-0.438	-0.332	-0.263	0.138	-0.425	0.853	0.012

Table 5.1: Calculated correlation coefficients and effective temperature of kagome lattice in Figure 5.2 d).

We compared the correlation coefficients from Table 5.2 with Monte Carlo simulations, and the result is shown in Figure 5.3 a). It would seem that we reach the SI2 phase – although we have an almost perfect ground state. This is caused by the defects on the edges. Therefore we analysed the image 5.2 d) again but only the vertices that lie within the red frame.

Results of the second analysis are shown in Table 5.2 and comparison of the experiment and Monte Carlo simulations are shown in Figure 5.3 b).

We were able to reach a ground state of the kagome lattice with notch depth 150 nm. This system is affected by the magnetic defects on the edges of the lattice – this problem would disappear with infinite size lattice. After we removed the defects on the edges, we acquire perfect ground state of the kagome lattice.

5.1. BRINGING THE DIPOLAR KAGOME ICE IN ITS GROUND STATE

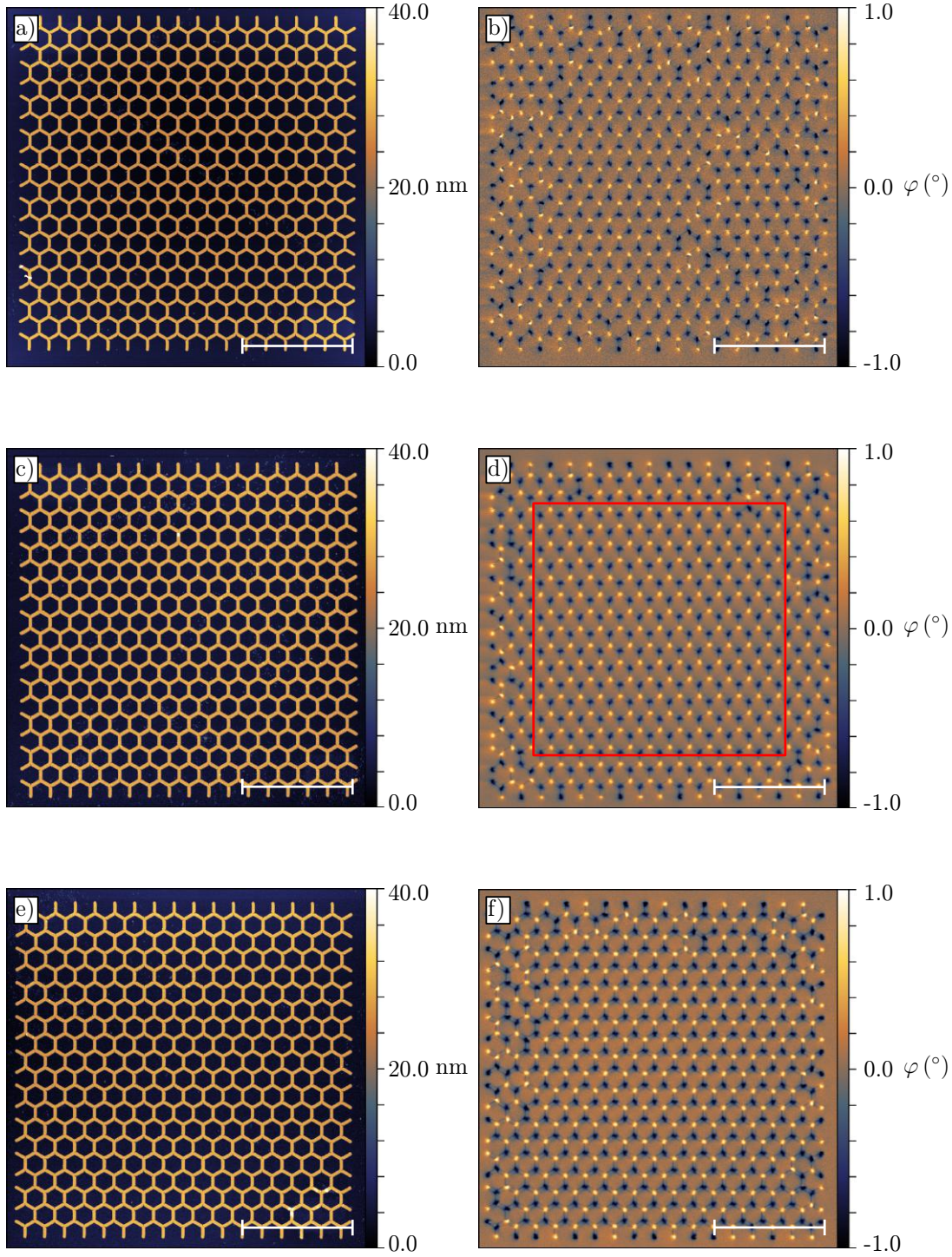


Figure 5.2: Lattices with the depth of the notch 150 nm after seven day demagnetization. The topography of the lattices acquired by AFM is shown in images a), c) and e) and their corresponding MFM signals are in images b), d) and f) and it can be seen that magnetic charge ordering is almost perfect through all lattices. White lines in the images represent the distance of $10\ \mu\text{m}$. Red frame in image d) marks the area from which spin-spin correlations was calculated to achieve results without defects on the edges.

Our demagnetization protocol is super efficient and therefore, we do not observe any domain wall in the bulk of our kagome lattice that would separate different patches of the ground state.

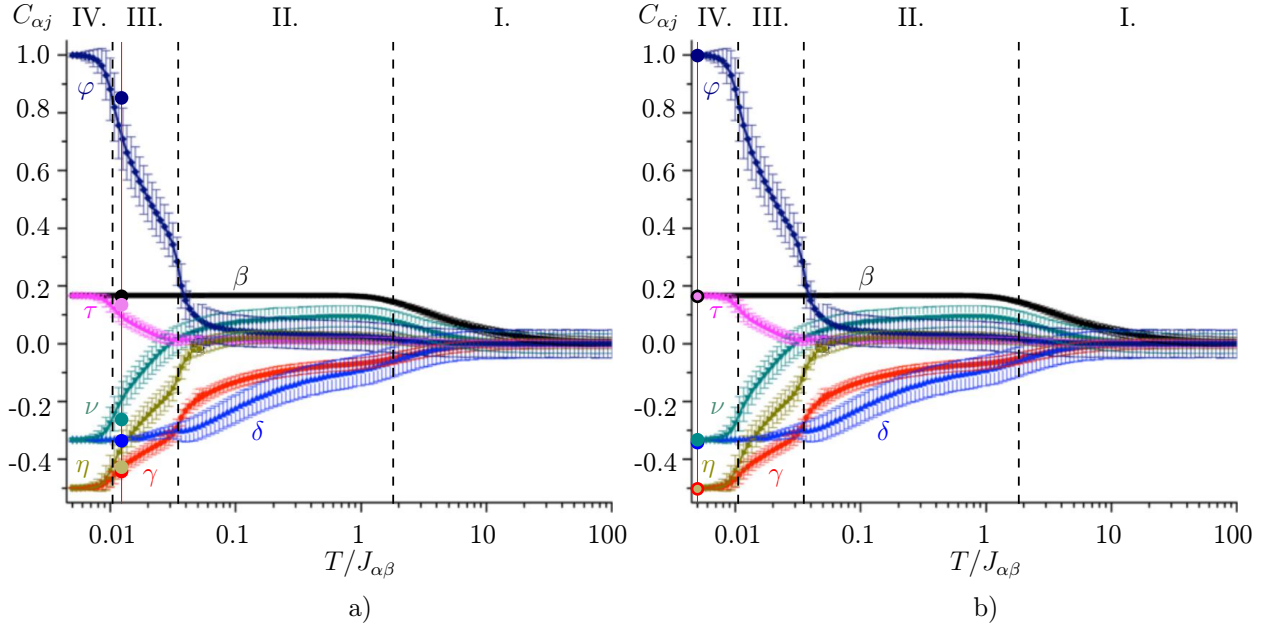


Figure 5.3: Pairwise spin correlations $C_{\alpha j}$ as a function of effective temperature $T/J_{\alpha\beta}$. The curves are deduced from Monte Carlo simulations and taken from [7]. The dots are experimental measurements. In a) experimental values were calculated from Figure 5.2 d) and the effective temperature is of the order of 0.012 a.u. b) experimental values were calculated from Figure 5.2 d) without the edges (vertices in the red frame only) and the effective temperature is of the order of 0.005 a.u. All correlation coefficients correspond to Monte Carlo predictions for a) SI2 phase and b) LRO phase.

Correlation coefficients $C_{\alpha j}$							Effective temperature $T/J_{\alpha\beta}$ (a.u.)
β	γ	δ	ν	τ	η	φ	
0.167	-0.500	-0.341	-0.342	0.167	-0.500	1.000	0.005

Table 5.2: Calculated correlation coefficients and effective temperature of kagome lattice in Figure 5.2 d) without the edges.

5.2. Towards the investigation of exotic, cooperative phenomena

Next step was to force the system to undergo a phase transition from LRO to SI2 or SI1. The energy of the system can be tuned by adjusting two parameters - demagnetization protocol length and notch depth. For the purpose of studying system in the phase SI2, we found notch depth of 50 nm and seven days demagnetization as most suitable parameters. The analysis was performed on four lattices of the same type. AFM image of one lattice of this type is shown in Figure 5.4 a), MFM images of the four analysed lattices are shown in Figure 5.4 b) – e). Correlation coefficients of the four lattices were averaged in order to get rid of the edge effect. Mean values of the correlation coefficients are shown in Table 5.3

Correlation coefficients indicate that these lattices are in SI1 phase as is visualised in Figure 5.5, where data from Table 5.3 are compared with Monte Carlo simulations for the effective temperature of 0.037 a.u. in Figure 5.5. We found good agreement with

5.2. TOWARDS THE INVESTIGATION OF EXOTIC, COOPERATIVE PHENOMENA

Monte Carlo simulations for all correlation coefficients. Based on analysis of correlation coefficients, the system is in deep SI1.

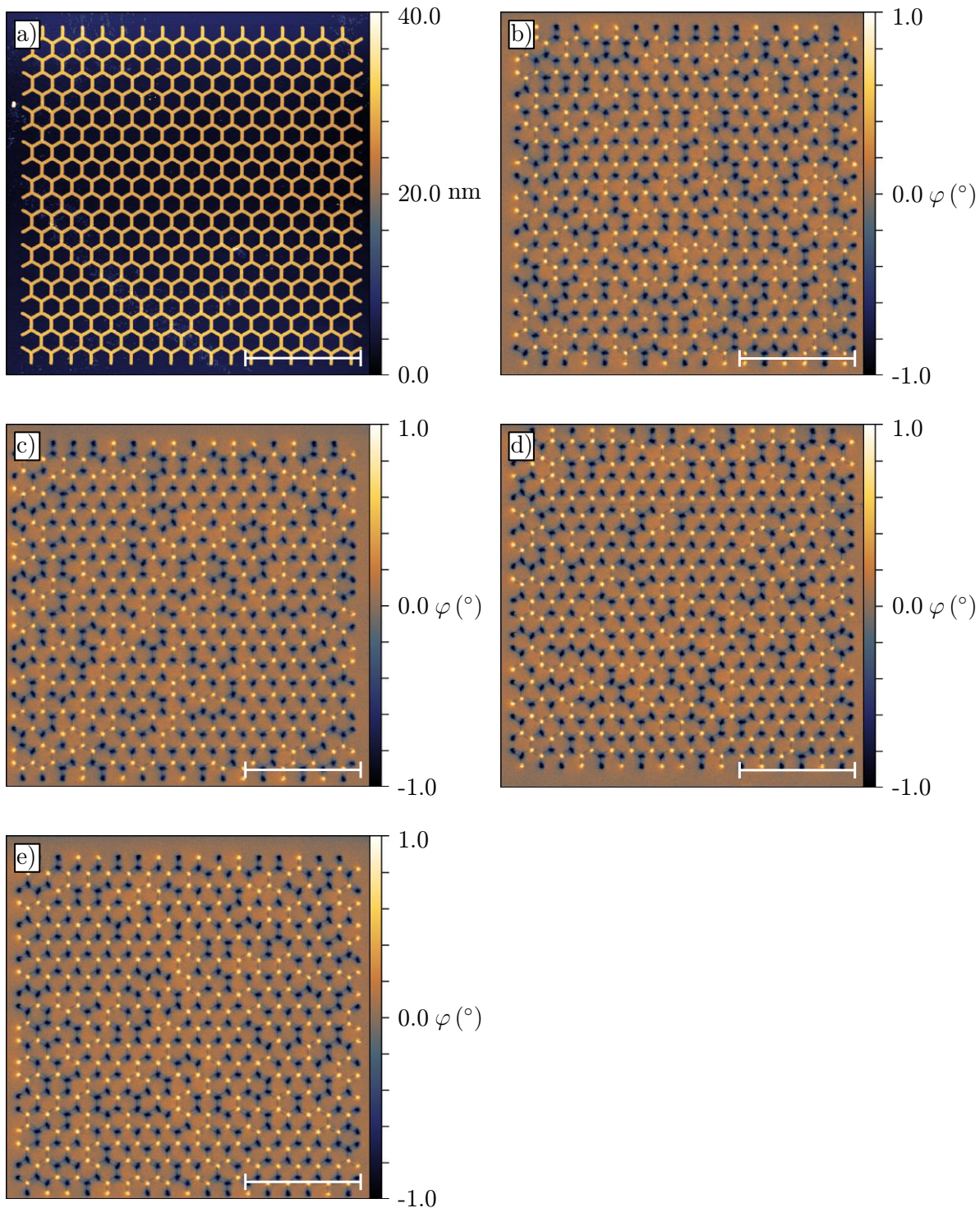


Figure 5.4: Lattices with the depth of the notch 50 nm after seven day demagnetization. The topography of one of the lattice acquired by AFM is shown in images a) Its corresponding MFM signals is in images b). Images c), d) and e) shows MFM signal of another three lattices. It can be seen that magnetic charge is much more disordered on these lattices than on lattices in Figure 5.2. White lines in the images represent the distance of $10 \mu\text{m}$.

Correlation coefficients $C_{\alpha j}$							Effective temperature $T/J_{\alpha\beta}$ (a.u.)
β	γ	δ	ν	τ	η	φ	
0.17	-0.20	-0.27	-0.03	0.02	-0.09	0,18	0.037
$\pm 0,00$	$\pm 0,05$	$\pm 0,03$	$\pm 0,07$	$\pm 0,03$	$\pm 0,07$	$\pm 0,12$	

Table 5.3: Mean value of correlation coefficients calculated from four different lattices and effective temperature, which was calculated from mean values of correlation coefficients of kagome lattices shown in Figure 5.4.

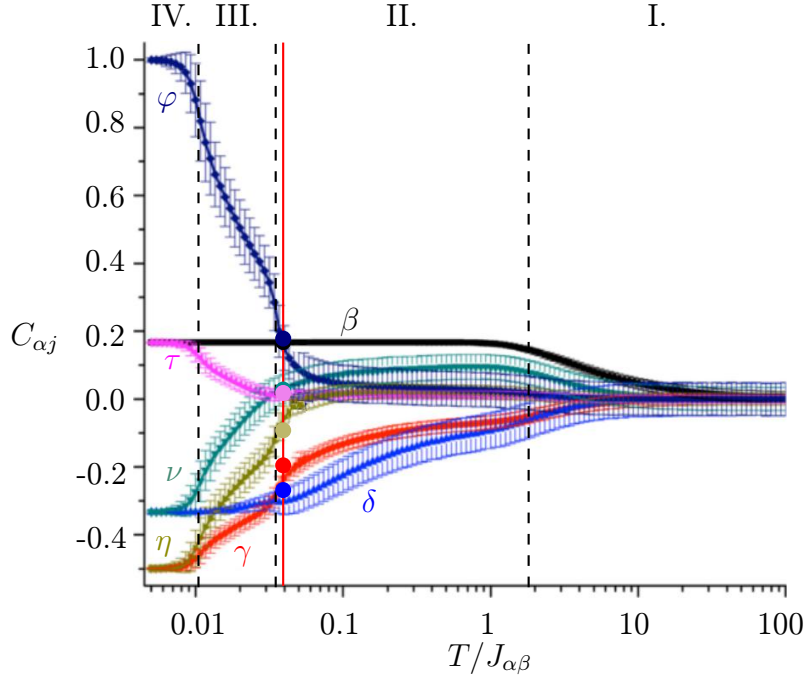


Figure 5.5: Pairwise spin correlations $C_{\alpha j}$ as a function of effective temperature $T/J_{\alpha\beta}$. The curves were obtained by Monte Carlo simulations and taken from [7]. The dots represent our experimental results. The effective temperature of the system is 0.037, and all correlation coefficients correspond to Monte Carlo predictions for deep SI1 phase.

Another method to determine the phase of the system is to test whether the system exhibits fragmentation – collective behaviour of the spins associated with the SI2 phase. If the fragmentation is present in the system, we can say that the collective state of matter emerges. Each single classical magnetic moment (macrospin) does two completely opposite things at the same time: it fluctuates and remains static. The magnetic moment is fragmented, i.e., is split into two distinct components.

A way to visualize the spin fragmentation is to plot the magnetic structure factor $S(q)$ associated with a given spin configuration. $S(q)$ is the Fourier transform of the spin correlations [4]. In the plot of magnetic structure factor, all static components of macrospin are revealed through magnetic Bragg peaks and the dynamic component of macrospins as a structured diffuse background signal [4, 5].

The magnetic structural factor of Monte Carlo simulations of the SI1 and SI2 phase can be seen in Figure 5.6 a) and c) respectively. These structural factors were calculated at Néel Institute, and the images were taken and modified from [17]. For all four lattices from Figure 5.4 b), c), d) and e), magnetic structural factor was calculated as well, and results are shown in Figure 5.6 b), d), e) and f) respectively.

5.2. TOWARDS THE INVESTIGATION OF EXOTIC, COOPERATIVE PHENOMENA

In Figure 5.6 we can see that structural factors in case of a) and b) are similar – there are no Bragg peaks, and diffused background dominates. On the other hand, structural factors in case of c), d), e) and f) shows Bragg peaks and less diffused background. For better orientation, some markers were added to the Figures. Circles of different colours mark positions where Bragg peaks occur. White and red frames mark positions where Bragg peaks would be if the system was in SI2 phase. These results indicate that lattices from Figure 5.4 c), d) and e) exhibit fragmentation, and therefore are in or close to SI2 phase.

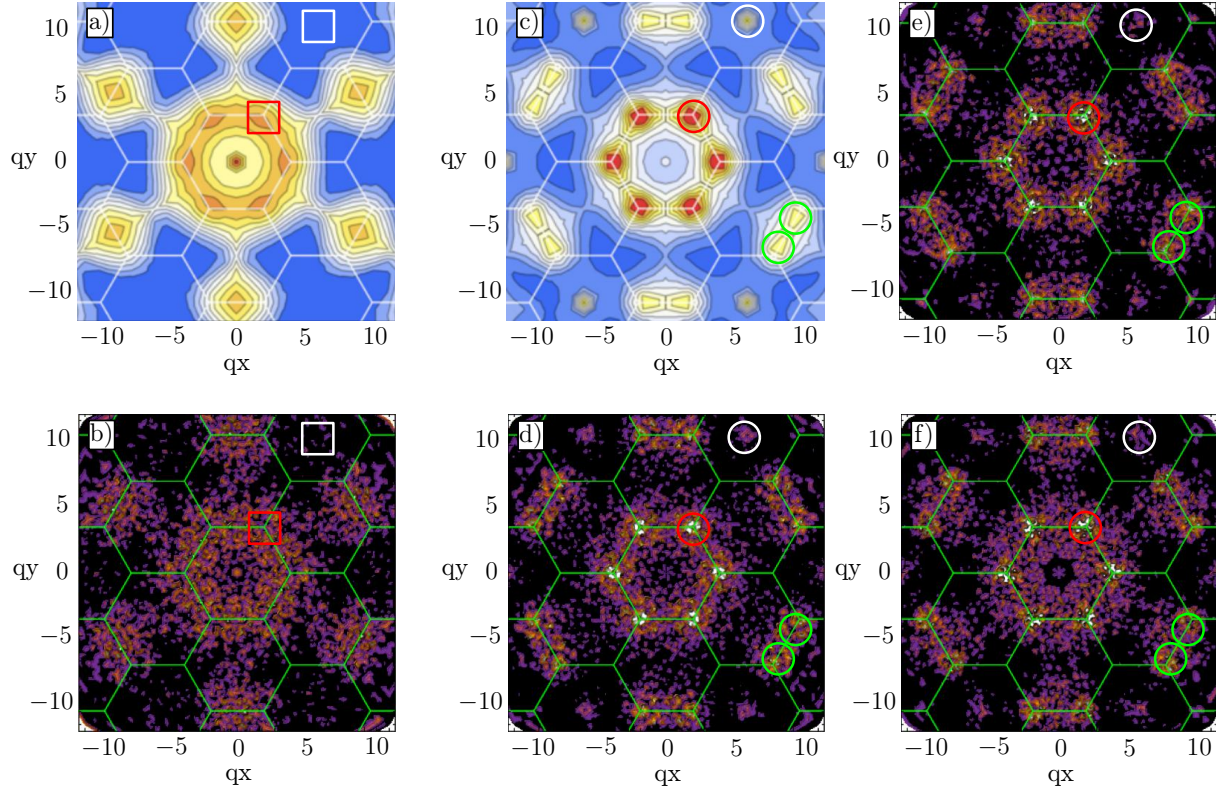


Figure 5.6: Magnetic structural factor of SI1 and SI2 phases calculated from Monte Carlo simulations are shown in a) and b) respectively. Images b), d), e) and f) show magnetic structural factor calculated from measured of lattices in Figure 5.4 b), c), d) and e) respectively. In each image the diffused background is visible, but in images d), e) and f) formation of Bragg peaks, in areas that are marked with colour circles, can be observed. Coexistence of Bragg peaks and diffused background indicate that lattices might be in SI2 phase where fragmentation of spins occur. On the other hand image b) do not show any Bragg peak in marked areas and is more similar to the magnetic structure factor of SI1 phase.

Based on correlation coefficient analysis and a magnetic structural factors, identifying the phase of the system is not conclusive. Correlation coefficient analysis may be affected by edge effects. On the other hand, based on magnetic structural factor, only three of four lattice exhibit fragmentation. The reasons we did not reach SI2 are following. First, the notches of the lattice may not be large enough to force the system to be in SI2 phases. Second, the transition to SI2 may require longer demagnetization protocol.

The SI2 phase might be reached by demagnetization of the sample for a longer time. However, based on my experience, it is very probable that lattice with the depth of the notch between 50 nm and 150 nm needs to be fabricated for observing clear SI2.

Nevertheless, we reached the lowest measured effective temperature for SI1. So far the best result by using demagnetization protocol was $T_n = 0.56$ a.u. [6].

To proclaim our modified lattice as a suitable tool for probing dipolar kagome spin ice model, we need to be able to excite some lattices into the state with higher effective temperature, in order to prove that even high energy phases can be captured.

To acquire high energy phases, measurements of five kagome lattices with the depth of the notch 50 nm after 10 second demagnetization protocol has been done. Outcomes of MFM measurement of these lattices are shown in Figure 5.7. Averaged correlation coefficients from these five lattices are shown in Table 5.4 along with an effective temperature of the system.

Comparison between the measured correlation coefficient from Table 5.4 and Monte Carlo simulation is shown in Figure 5.8. Results of the measurement on lattices with depth of the notch 50 nm after 10 second demagnetization protocol show us that we are able to reach even regular SI1 phases.

Correlation coefficients $C_{\alpha j}$							Effective temperature $T/J_{\alpha\beta}$ (a.u.)
β	γ	δ	ν	τ	η	φ	
0.17	-0.14	-0.22	0.05	0.01	0.00	0.04	0.106
$\pm 0, 00$	$\pm 0, 02$	$\pm 0, 03$	$\pm 0, 03$	$\pm 0, 013$	$\pm 0, 03$	$\pm 0, 07$	

Table 5.4: Mean value of correlation coefficients calculated from five different lattices and effective temperature, which was calculated from mean values of correlation coefficients, of kagome lattices shown in Figure 5.7.

Because we were able to probe LRO phase, deep SI1 and SI1 phase with our lattices, we believe that our modified lattices are a suitable tool to measure and probe exotic phase of artificial dipolar kagome spin ice systems.

5.2. TOWARDS THE INVESTIGATION OF EXOTIC, COOPERATIVE PHENOMENA

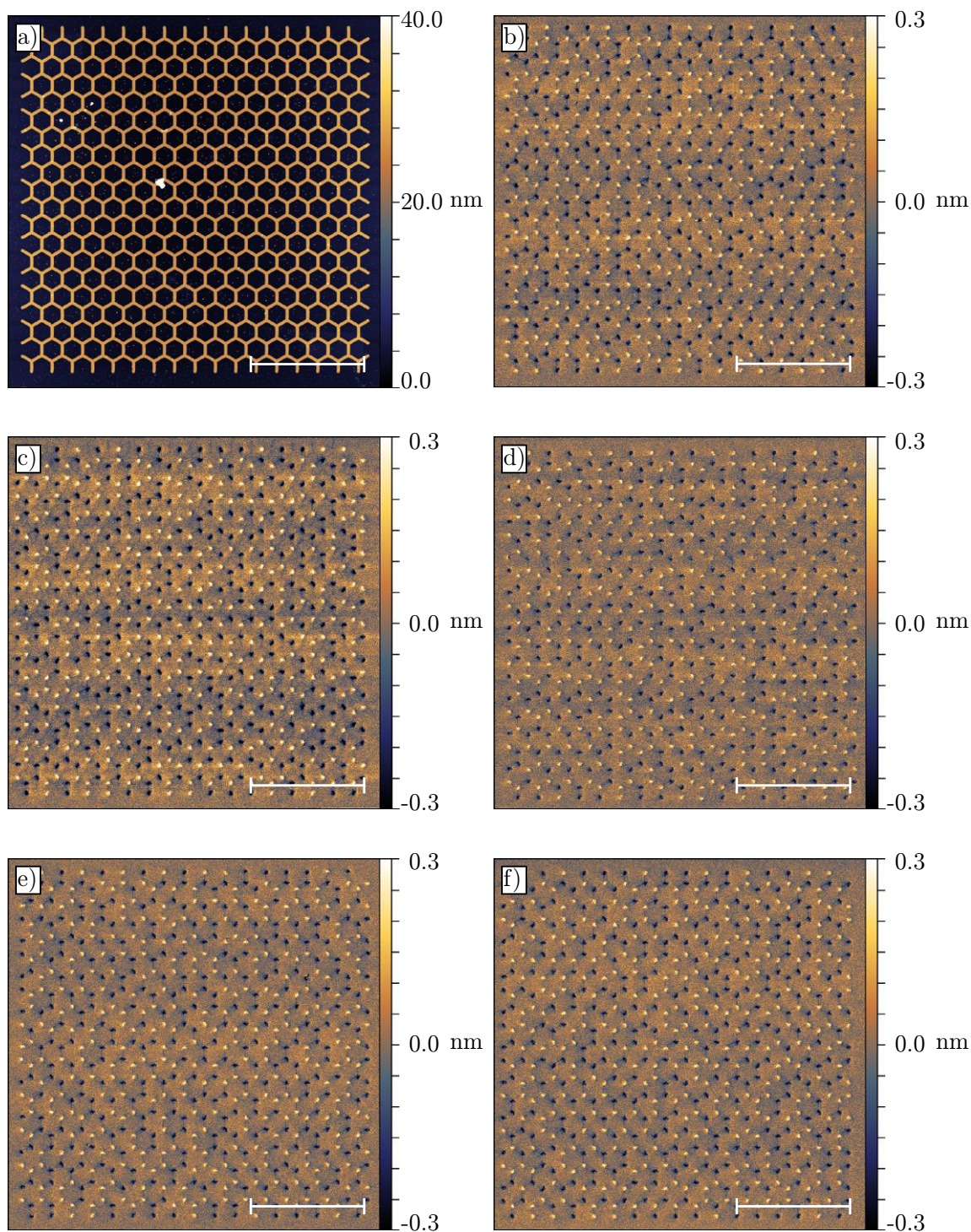


Figure 5.7: Lattices with the depth of the notch 50 nm after 10 seconds demagnetization. The topography of one of the lattices acquired by AFM is shown in images a) Its corresponding MFM signals is in images b). Images c), d) and e) shows MFM signal of another three lattices. It can be seen that magnetic charge is much more disordered on these lattices that on lattices in Figure 5.2. White lines in the images represent the distance of $10 \mu\text{m}$.

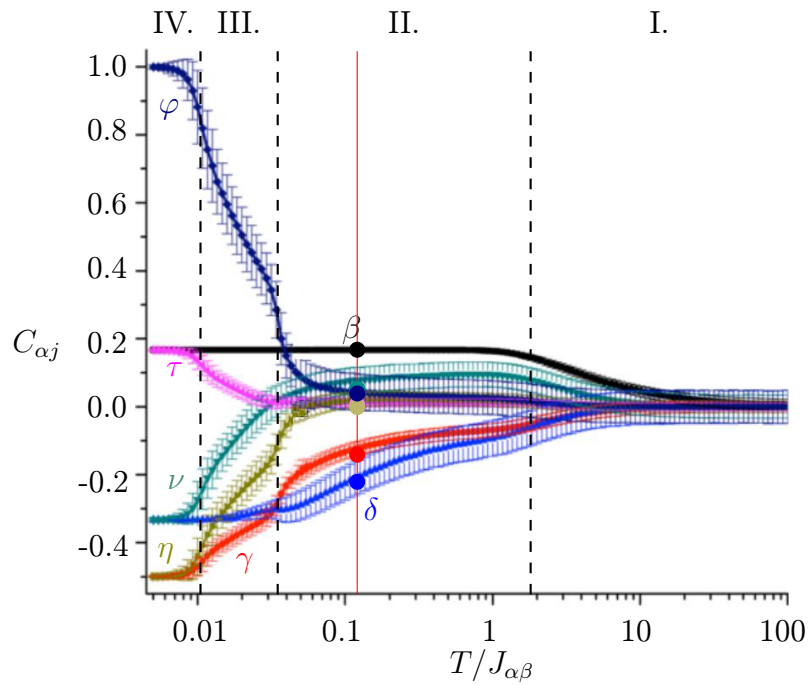


Figure 5.8: Pairwise spin correlations $C_{\alpha j}$ as a function of effective temperature $T/J_{\alpha\beta}$. The curves are deduced from Monte Carlo simulations and taken from [7]. The dots are mean values of experimental measurements. The effective temperature of the system is 0.106, and all correlation coefficients correspond to Monte Carlo predictions for SI1 phase.

6. Concluding remarks

The goal of this work was to modify kagome lattice that would be more suitable as a tool for studying low energy exotic phases and phenomena such as the collective behaviour of the spins in the matter. So far the attempts to explore and measure low energy physics of kagome systems were made by lowering the effective temperature of the system by demagnetization protocols or thermal annealing. Due to the dynamics of the system, it was very hard to reach the exotic physics that is predicted. Most of the time the system gets trapped in a state with high effective temperature.

In this work, we present a different approach. Instead of trying to lower the effective temperature of the system to reach the low energy physics, we go another way around. We modified the lattice by using strategically placed defects. These defects cause that the system is trapped in the ground state.

With our lattices, we were able to reach the ground state repeatedly simply by applying demagnetization protocols. And we managed to observe perfect ground state configuration on a large kagome lattice.

We found out the way how to tune the effective temperature of the system almost at will by optimizing two key parameters. The first parameter is length (efficiency) of the demagnetization protocol – to reach lower effective temperature we need to use longer demagnetization protocol. The second parameter is the size of the defect in the lattice. Bigger defects force the system into the lower effective temperature.

By changing defect size and length of demagnetization protocol, we were able to probe phase diagram of our lattices. We observed both low and high energy configuration of kagome lattice. Each probed configuration corresponds perfectly to the theoretical predictions and we were able to experimentally observe the fragmentation. Therefore it is confirmed that our lattices are usable for probing exotic phases of dipolar kagome spin ice model.

Another goal was to develop software for analysis of MFM measurement. This software was programmed in LabVIEW. It is user-friendly and provides a faster way how to analyse the magnetic signal from large-scale kagome lattices.

7. Bibliography

- [1] W. Giauque and M. Ashley, “Molecular rotation in ice at 10°k. free energy of formation and entropy of water,” *Physical Review*, vol. 43, 1933.
- [2] L. Pauling, “The structure and entropy of ice and of other crystals with some randomness of atomic arrangement,” *Journal of the American Chemical Society*, vol. 57, 1935.
- [3] E. Saitoh *et al.*, “Domain-wall trapping in a ferromagnetic nanowire network,” *Journal of Applied Physics*, vol. 93, 2003.
- [4] M. E. Brooks-Bartlett *et al.*, “Magnetic-moment fragmentation and monopole crystallization,” *Physical Review*, vol. 4, 2014.
- [5] B. Canals *et al.*, “Fragmentation of magnetism in artificial kagome dipolar spin ice,” *Nature Communications*, vol. 7, 2016.
- [6] I. A. Chioar *et al.*, “Kinetic pathways to the magnetic charge crystal in artificial dipolar spin ice,” *Physical Review B*, vol. 90, 2014.
- [7] I. A. Chioar *et al.*, “Nonuniversality of artificial frustrated spin systems,” *Physical Review B*, vol. 90, 2014.
- [8] C. L. Henley, “The coulomb phase in frustrated systems,” *Annual Review of Condensed Matter Physics*, vol. 1, 2010.
- [9] R. F. Wang *et al.*, “Artificial spin ice in a geometrically frustrated lattice of nanoscale ferromagnetic islands,” *Nature*, vol. 439, 2006.
- [10] H. G. Wannier, “Antiferromagnetism. the triangular ising net,” *Physical Review*, vol. 79, 1950.
- [11] A. D. McNaught *et al.*, *IUPAC. Compendium of Chemical Terminology*. Oxford: Blackwell Scientific Publications, 2. ed., 1997.
- [12] R. Kalousek, *Jemný úvod do statistické fyziky a termodynamiky*. electronic textbook, 2014.
- [13] A. Y. Klimenko, “Teaching the third law of thermodynamics,” *The Open Thermodynamics Journal*, vol. 6, 2012.
- [14] A. P. Ramirez *et al.*, “Zero-point entropy in spin ice,” *Nature*, vol. 399, 1999.
- [15] R. Siddharthan *et al.*, “Ising pyrochlore magnets: Low-temperature properties, ice rules, and beyond,” *Physical Review Letters*, vol. 83, 1999.
- [16] J. Cumings *et al.*, “Focus on artificial frustrated systems,” *New Journal of Physics*, vol. 16, 2014.
- [17] N. Rougemaille, “Cooperative magnetic phenomena in artificial spin systems: spin liquids, coulomb phase and fragmentation of magnetism,” *manuscript*, 2018.

- [18] J. D. Bernal and R. Fowler, “A theory of water and ionic solution, with particular reference to hydrogen and hydroxyl ions,” *The Journal of Chemical Physics*, vol. 1, 1933.
- [19] R. Stamps, *Solid State Physics*. Academic Press, 1. ed., 2016.
- [20] M. J. Harris *et al.*, “Geometrical frustration in the ferromagnetic pyrochlore $\text{Ho}_2\text{Ti}_2\text{O}_7$,” *Physical Review Letters*, vol. 79, 1997.
- [21] I. Gilbert *et al.*, “Emergent ice rule and magnetic charge screening from vertex frustration in artificial spin ice,” *Nature Physics*, vol. 10, 2014.
- [22] S. Blundell, *Magnetism in condensed matter*. New York: Oxford University Press, 1. ed., 2001.
- [23] N. Rougemaille *et al.*, “Artificial kagome arrays of nanomagnets: A frozen dipolar spin ice n.,” *Physical Review Letters*, vol. 106, 2011.
- [24] Y. Perrin, B. Canals, and N. Rougemaille, “Extensive degeneracy, coulomb phase and magnetic monopoles in artificial square ice,” *Nature*, vol. 540, 2016.
- [25] V. Schánilec *et al.*, “Artificial vertex systems by design,” *manuscript under review*, 2017.
- [26] M. Tanaka, E. Saitoh, and H. Miyajima, “Magnetic interactions in a ferromagnetic honeycomb nanoscale network,” *Physical Review B*, vol. 73, 2006.
- [27] S. Petit *et al.*, “Observation of magnetic fragmentation in spin ice,” *Nature Physics*, vol. 12, 2016.
- [28] L. Anghinolfi *et al.*, “Thermodynamic phase transitions in a frustrated magnetic metamaterial,” *Nature Communications*, vol. 6, 2015.
- [29] J. C. Gartside *et al.*, “Realization of ground state in artificial kagome spin ice via topological defect-driven magnetic writing,” *Nature Nanotechnology*, vol. 13, 2018.
- [30] A. Vansteenkiste *et al.*, “The design and verification of MuMax³,” *American Institute of Physics*, vol. 4, 2014.
- [31] P. Etalon and P. West, *Atomic Force Microscopy*. Oxford University Press, 1. ed., 2010.
- [32] U. Hartmann, “Magnetic force microscopy,” *Annual Review of Materials Science*, vol. 29, 1999.
- [33] S. Porthun, L. Abelmann, and C. Lodder, “Magnetic force microscopy of thin film media for high density magnetic recording,” *Journal of Magnetism and Magnetic Materials*, vol. 182, 1997.
- [34] V. L. Mironov, *Fundamentals of scanning probe microscopy*. The Russian Academy of Sciences Institute, 1. ed., 2004.

7. BIBLIOGRAPHY

- [35] R. F. Wang *et al.*, “Demagnetization protocols for frustrated interacting nanomagnet arrays,” *Journal of Applied Physics*, vol. 101, 2007.
- [36] X. Ke *et al.*, “Energy minimization and ac demagnetization in a nanomagnet array x,” *Physical Review Letters*, vol. 101, 2008.
- [37] A. Schumann *et al.*, “Charge ordering of magnetic dipoles in artificial honeycomb patterns,” *Applied Physics Letters*, vol. 97, 2010.

8. Acronyms

AF	Antiferromagnetic
AFM	Atomic force microscopy
ASI	Artificial spin ice
EBL	Electron beam lithography
FM	Ferromagnetic
GS	ground state
IAAS	Image auto-analysis software
IPA	Isopropyl alcohol
LRO	Long range order
LS	Left-sided magnetic configuration of the vertex
MFM	Magnetic force microscopy
RS	Right-sided magnetic configuration of the vertex
SEM	Scanning electron microscopy
SI	Spin ice
SI1	Spin ice I. phase of dipolar kagome spin ice system
SI2	Spin ice II. phase of dipolar kagome spin ice system